ANL-6221
Reactors - General
(TID-4500, 15th Ed.)
AEC Research and
Development Report

ARGONNE NATIONAL LABORATORY
9700 South Cass Avenue
Argonne, Illinois

THEORETICAL FEEDBACK ANALYSIS IN BOILING WATER REACTORS

by

A. Ziya Akcasu*
Reactor Engineering Division

October 1960

*Including work done by F. Velona (Senn, Italy)

Operated by The University of Chicago
under
Contract W-31-109-eng-38

DISCLAIMER

TABLE OF CONTENTS

LIST OF FIGURES

LIST OF TABLES

NOMENCLATURE

A	Channel cross-sectional area
A_d	Downcomer cross-sectional area
$A_s(x,t)=A_s^0(x) + a_s(x,t)$	Steam cross-sectional area
$A_w(x,t)=A_w^0(x) + a_w(x,t)$	Water cross-sectional area
B	Friction coefficient
C_1, C_2	Friction coefficients in the nonboiling and boiling regions
c_1, c_2, c_w	Specific heats of fuel section, cladding and water
$D(x)$	Flux distribution function
d_1, d_2	Half-thickness of the fuel section and the thickness of the cladding
g	Acceleration due to gravity
$H(x,t)=H^0(x) + h(x,t)$	Enthalpy of subcooled water
H_{fw}	Enthalpy of feedwater
H_s	Saturation enthalpy of steam
$H_w(t)=H_w + h_w(t)$	Saturation enthalpy of water
H_v	Latent heat per unit volume of steam
$K(x)$	See Eq.(42)
$K_1(x), K_2(x)$	See Eqs.(47) and (48)
k_1, k_2	Thermal conductivities of the fuel and cladding materials
L	Reduced core height
L'	Actual core height
L_{nb}	Length of nonboiling region
L_b, L_b'	Reduced and actual length of the boiling region
L_c	Length of the chimney
M_w	Water mass in the vessel
M_s	Steam mass in the vessel
M_d, M_{nb}	Masses of water in the downcomer and in the nonboiling region

M_b	Total mass in the boiling region (water + steam)
$\dot{M}_{fw}, \dot{m}_{fw}$	Steady state and incremental feedwater mass flow rates
$\dot{M}_r$	Mass flow rate of the recirculating water
$\dot{M}_t = \dot{M}_r + \dot{M}_{fw}$	Total water flow rate in the core
$N(t) = N^0 + n(t)$	Nuclear power
$P(t) = P^0 + p(t)$	Pressure
P_f, P_i	Frictional and inertial forces
$Q(t) = Q^0 + q(t)$	Total thermal power supplied to the channel
$Q(x,t) = Q^0(x) + q(x,t)$	Thermal power per unit height of channel
R_1, R_2, R_3	Thermal resistances of the half fuel section, the cladding and the film
T_r	Recirculation time
T_s, T_w	Steam and water transit times
$U(x,t) = U^0(x) + u(x,t)$	Steam velocity
$U_p(x)$	Steam perturbation velocity
U_0	Average steam velocity in the boiling region
U_1, U_2	Steam velocities at the boiling boundary and at the core outlet
$V(t) = V^0 + v(t)$	Total steam volume in the core
$V_n(t) = V_n^0 + v_n(t)$	Net steam volume in the core
V_f	Volume of the fuel plates
$W(x,t) = W^0(x) + w(x,t)$	Water velocity in the boiling region
$W_0(t) = W_0^0 + w_0(t)$	Water velocity in the nonboiling region

GREEK SYMBOLS

α, β	$(\pi L_b/L)$ and $(\pi L_{nb}/L)$
$\delta(t)$	Boiling boundary shift
$\Theta(t) = \Theta^0 + \theta(t)$	Temperature drop across the film

θ_s	Saturation temperature
$\theta_w(x,t)$	Incremental water temperature in the nonboiling region
Σ	Total momentum in the circulation loop
$\theta_w(t)$	Incremental water temperature (averaged in the whole channel)
$\theta_f(x,t)$	Incremental fuel temperature (averaged transversally at x)
$\theta_f(t)$	Incremental fuel temperature (averaged in the whole fuel plate)
$\nu(x,t)$	Nuclear power generated in the half fuel section per unit surface area
$\rho_1, \rho_2, \rho_s, \rho_w$	Densities of fuel material, cladding, steam and water
τ_1, τ_2	$(\rho_1 c_1 d_1^2/k_1)$ and $(\rho_2 c_2 d_2^2/k_2)$
$\tau_d, \tau_f, \tau_{pv}, \tau_{qw}, \tau_{qb}$	Time constants (see Section XII)
τ	Time lag due to the steam formation
τ_{max}	Bubble growth time
$\Psi(x,t)=\Psi^0(x) + \psi(x,t)$	Heat flow per unit surface
ω_s, ω_w	(α/T_s) and (β/T_w)

THEORETICAL FEEDBACK ANALYSIS IN BOILING WATER REACTORS

by

A. Ziya Akcasu

ABSTRACT

The dynamic behavior of boiling water reactors for small perturbations was investigated in a systematic way. General expressions for the transfer functions associated with the individual feedback mechanisms were obtained for an arbitrary flux distribution, weighting function, and steam velocity distribution. Specific forms were derived in the case of a first power flux weighting, a uniform steam velocity distribution, and a sinusoidal flux distribution with an adjustable wave length. These forms were simplified and single time-constant transfer functions were obtained. The error involved in the lumped time-constant approximation was shown to be as large as 4 db in amplitude in certain feedback mechanisms. Theoretical results were applied to the experimental power-void transfer function obtained at Ramo-Wooldridge Research Laboratory, and to the EBWR transfer function. In the former case, the agreement was found to be reasonably good, but yet more systematic experimental data were needed to reach a definite conclusion as to the validity of the proposed model, which assumes a time lag associated with steam formation and a steam perturbation speed greater than the steady-state steam velocity. In the second application, the agreement between the experimental and calculated reactor responses was proved to be better than 5 decibels in amplitude and 10 degrees in phase, in the entire frequency range from 0.01 to 100 rad/sec.

I. INTRODUCTION

This report contains an analysis of the inherent nuclear feedback in boiling water reactors. The objective is to obtain a quantitative understanding of the various feedback mechanisms in boiling reactors. The analysis is based on the linearized treatment by means of Laplace transforms of the nonlinear differential equations describing the reactor system. The validity of the theory is therefore restricted to small variations

about the steady-state values of the reactor parameters. Separate treatment of the individual feedback mechanisms is allowed on the ground of superposition principle.

The method of analysis consists of the following steps:

a. The transfer functions associated with each feedback mechanism are derived in an integral form for any flux and steam-velocity distribution, and for any reactivity weighting function (horizontal flux variation and thus horizontal weighting are not considered). These general forms may be used for numerical investigations if the above three functions are experimentally known.

b. By evaluating the integrals in the case of uniform steam velocity, sinusoidal flux distribution and first-power flux weighting, analytical expressions are obtained for each transfer function.

c. These analytical forms are further simplified, and the approximate expressions with a single time constant are derived. The validity of the single time-constant approximation is checked by comparing the amplitude responses of the original and approximated transfer functions.

The assumptions made in the second step for obtaining specific forms of the transfer functions require further consideration. The assumption of sinusoidal flux distribution becomes fairly realistic when a "reduced" core height is introduced to take into account the flux depression near the top of the core due to the presence of steam. The assumption of first-power flux weighting requires more apology since the change in the local diffusion coefficient due to the voids is weighted with respect to the square of the flux gradient, and the change in the absorption is weighted with the square of the flux itself (one-group theory). First-order flux weighting for the combined effect may therefore be expected to be qualitatively correct. Nevertheless, it is more realistic than completely ignoring the weighting phenomenon. As to the steam-velocity distribution, the following argument may be given: It is found that the time constants associated with various transients in the boiling region turn out to be proportional to the steam-transit time, with a proportionality constant which depends only on the ratio of the boiling and nonboiling lengths. It may be expected that the value of this constant of proportionality will not be too sensitive to a particular steam-velocity distribution.

The presented report stems from the work by E.S. Beckjord.[1] Therefore, it is regarded by the author as a second step towards a better understanding of the dynamic behavior of boiling water reactors.

II. HEAT TRANSFER IN FUEL PLATES

The heat released in the fuel section by the nuclear fission is transferred to the coolant through the fuel, the cladding, and the film between the fuel plate and the coolant. Therefore, it is appropriate to distinguish between the nuclear power N(t), generated in the fuel, and the heat power Q(t) supplied to the coolant. The purpose of this section is to establish the relation betweenN(t) and Q(t).

The heat transfer problem encountered here can be simplified by the following assumptions, which are realistic for a thin fuel plate whose thickness is small compared to its width and length:

(a) Heat flow in the x and z directions is ignored (see Fig. 1).

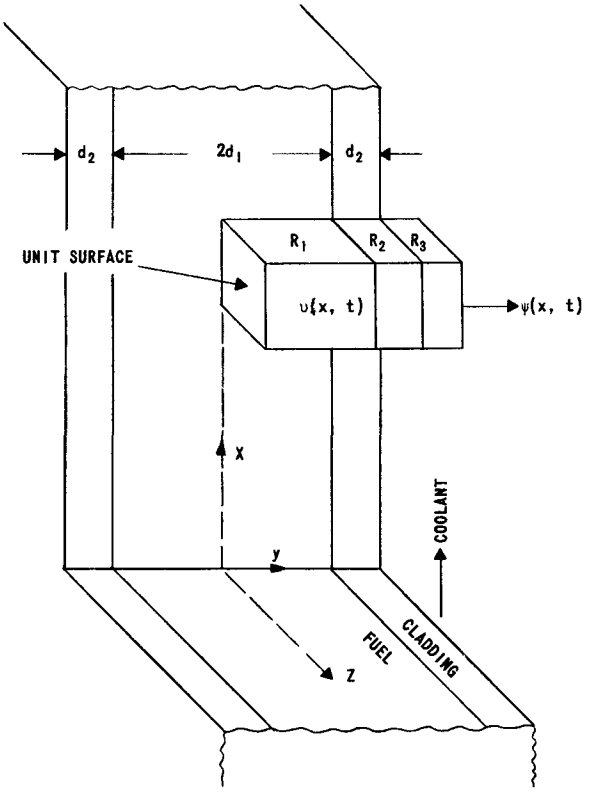

FIG. 1
HEAT TRANSFER IN FUEL PLATES

(b) The rate of heat production is uniform in the fuel.

(c) The temperature of the coolant is constant.

(d) The temperature variations are sufficiently small to allow the linearization of the film resistance. The latter is then defined as

$$\frac{1}{R_{3b}} = \left(\frac{\partial \Psi}{\partial \Theta}\right)_{\Theta = \Theta^0} \quad , \tag{1}$$

where Ψ is the heat flux and Θ is the temperature difference across the film. An explicit form of R_{3b} can be obtained from[2]

$$\Psi = 2.55 \times 10^{-4} e^{-0.0654 P} \Theta^4 \quad , \tag{2}$$

where Ψ, P (the pressure) and Θ are in watts/cm^2, atm and °C, respectively. Thermal resistance of the film follows from Eqs. (1) and (2) as

$$R_{3b} = \Theta^0 / 4\Psi^0 \quad . \tag{3a}$$

In the nonboiling region, the Dittus-Boelter equation[2,3] can be used to calculate R_{3nb} as the inverse of the heat transfer coefficient:

$$Nu = 0.023 \, Re^{0.8} \, Pr^{0.4} \quad , \tag{3b}$$

where Nu, Re, and Pr are the Nusselt, Reynolds and Prandtl numbers, respectively.

The solution of the heat transfer problem with the above assumptions is straightforward and can be found elsewhere.[4,5] If the Laplace transform is used, the final solution is obtained as

$$\frac{\overline{\nu}(x,s)}{\overline{\psi}(x,s)} = \frac{\tau_1 s}{R_1}\left(\frac{R_2}{\sqrt{\tau_2 s}} \sinh\sqrt{\tau_2 s} + R_3 \cosh\sqrt{\tau_2 s}\right) + \sqrt{\tau_1 s}$$

$$\left(\cosh\sqrt{\tau_2 s} + \frac{R_3}{R_2}\sqrt{\tau_2 s} \sinh\sqrt{\tau_2 s}\right) \coth\sqrt{\tau_1 s} \quad , \tag{4}$$

where $\overline{\nu}(x,s)$ and $\overline{\psi}(x,s)$ denote the Laplace transforms of the incremental nuclear power produced in the half fuel section per unit surface area (see Fig. 1) and the heat flux rate, respectively. The meanings of the other symbols in Eq. (4) are given in the nomenclature.

One observes that, except R_3, all the parameters on the right side of Eq. (4) are independent of x. Therefore, by ignoring the variation of R_3 or by defining an average R_3, one may replace $\overline{\psi}(x,s)$ and $\overline{\nu}(x,s)$ by $\overline{q}(s)$ and $\overline{n}(s)$, which are the incremental values of the total heat flow and the nuclear power, respectively.

By expanding the right-hand side of Eq. (4) into a Taylor series and retaining only the first and the second terms, one obtains

$$\frac{\bar{q}(s)}{\bar{n}(s)} = \frac{1}{1 + s\tau_f} \quad , \tag{5}$$

where

$$\tau_f = \tau_1 \left[\frac{R_2+R_3}{R_1} + \frac{1}{3} + \frac{\tau_2}{\tau_1}\left(\frac{1}{2} + \frac{R_3}{R_2}\right)\right] \quad . \tag{6}$$

If the method of eigenfunctions is used, the final solution is obtained as an infinite series:

$$\frac{\bar{q}(s)}{\bar{n}(s)} = \sum_{1}^{\infty} \frac{C_n}{1 + (s/\lambda_n)} \quad , \tag{7}$$

where the C_n are constants depending on the geometry of the two-region slab and on the thermal properties of the fuel and cladding; the λ_n are the roots of the following equation:

$$\tan\sqrt{\tau_1\lambda} = -\frac{k_2 d_1}{k_1 d_2}\sqrt{\frac{\tau_2}{\tau_1}}\,\frac{d_2 \cos\sqrt{\tau_2\lambda} - R_3 k_2 \sqrt{\tau_2\lambda}\,\sin\sqrt{\tau_2\lambda}}{d_2 \sin\sqrt{\tau_2\lambda} + R_3 k_2 \sqrt{\tau_2\lambda}\,\cos\sqrt{\tau_2\lambda}} \,, \tag{8}$$

which reduces to

$$\tan\sqrt{\tau_1\lambda} = -\frac{d_1}{R_3 k_1}\,\frac{1}{\sqrt{\tau_1\lambda}} \tag{9}$$

when the cladding is disregarded. Note that Eq. (8) can also be obtained from Eq. (4) by replacing s by $j\lambda$ and by equating the right side to zero.

The advantage of Eq. (7) over Eq. (4) is that it directly gives all the time constants, viz., $(1/\lambda_n)$, as the roots of a trigonometric equation. The previous method, however, yields the transfer function in a compact form rather than as a series and, thus, enables one to calculate the exact transfer function.

The single-time-constant approximation is obtained by retaining only the first term in Eq. (7). The remaining terms of the series decrease rapidly with increasing n. The gain of this approximate transfer function, viz., C_1, should be replaced by unity in order to obtain the exact zero-frequency response. Note that $\Sigma C_n = 1$.

It follows that both methods yield the same approximate form, namely, Eq. (5). The time constant τ_f can be evaluated either from Eq. (6) or from Eq. (8) in a given application, since both equations yield approximately the same numerical value. In fact, Eq. (6) represents an approximation by which to calculate the lowest root of the transcendental equation in Eq. (8).

Amplitudes of the exact and approximate transfer functions have been calculated from Eqs. (4) and (5), respectively, using the numerical values for EBWR at 20 Mw and 41 atm operation. The results are plotted in Fig. 2. It is observed that the single-time-constant approximation is quite satisfactory up to 25 rad/sec.

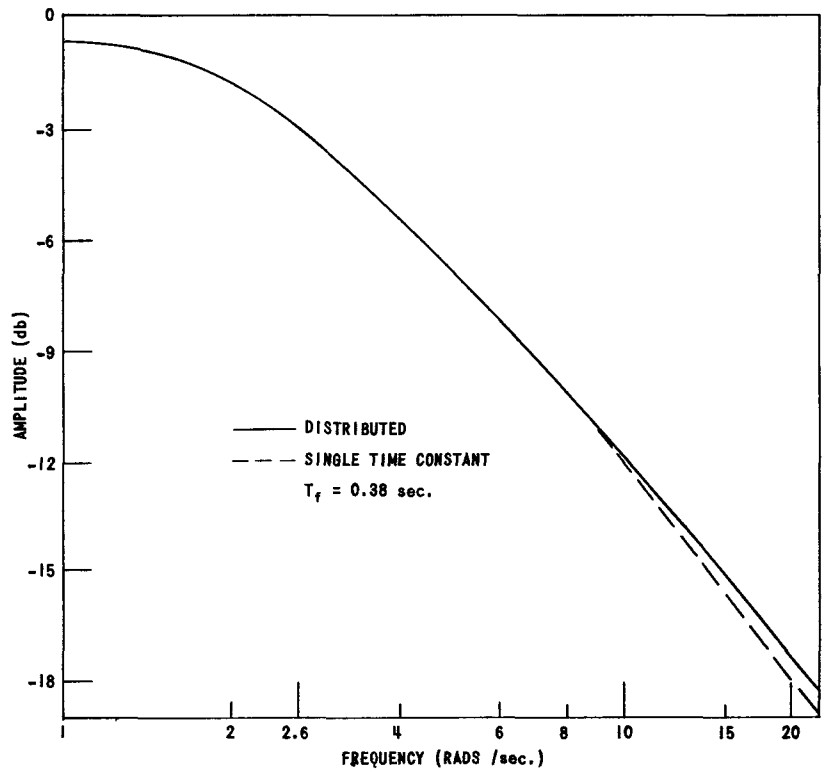

FIG. 2
AMPLITUDE RESPONSE OF FUEL PLATE TRANSFER FUNCTION

The following remarks seem to be in order:

(a) The frequency region, in which the single-time-constant approximation is valid, may not contain all the frequencies of interest for the kinetic studies. This point should be verified by plotting the amplitude (or phase) of the exact transfer function. If necessary, more than one time constant should be considered. In the latter case, the method of eigenfunctions proves to be more convenient.

(b) The value of the single time constant depends on the power level as well as on the pressure, because R_{3b} varies with power and pressure. The variation of R_{3b} with power is obtained from Eqs. (2) and (3a) as

$$R_{3b}^{x} = R_{3b}^{0} \left(Q^{0}/Q^{x}\right)^{\frac{3}{4}} \quad ,$$

where Q^0 and Q^x are the power levels corresponding to R^0_{3b} and R^x_{3b}. One observes that R_{3b}, and thus τ_f, will decrease with increasing power for a constant pressure. The variation of R_{3b} with pressure is obtained as

$$R^x_{3b} = R^0_{3b} \exp [(P^0 - P^x)/900] \quad .$$

Hence, R_{3b} and τ_f decrease with the increasing pressure. Experimental curves given in Reference 6, p. 29, support the predicted trend for the power variation.

(c) The time constant τ_f will have slightly different values in the boiling and nonboiling regions, due to the different character of the cooling in these two regions. This difference becomes negligible in the case of ceramic oxide fuel elements, due to the large value of R_1 as compared with R_3.

III. FUNDAMENTAL EQUATIONS OF MODERATOR DYNAMICS

The analysis of the moderator dynamics is essentially based on the conservation of both mass and energy. The former yields the following equation, when it is applied to a volume element of thickness dx along the channel:

$$\frac{\partial(A_s \rho_s U + A_w \rho_w W)}{\partial x} + \frac{\partial(A_s \rho_s + A_w \rho_w)}{\partial t} = 0 \quad . \tag{10}$$

The conservation of energy results in[7]

$$\frac{\partial(\rho_s A_s H_s U + \rho_w A_w H_w W)}{\partial x} + \frac{\partial(\rho_s A_s H_s + \rho_w A_w H_w)}{\partial t} = Q(x,t) \quad , \tag{11}$$

if (a) the variation of the kinetic and potential energies, and (b) the pressure change along the channel are neglected. The second assumption enables one to use enthalpy instead of internal energy.

In addition to (a) and (b), the following assumptions have been made throughout this report: (c) saturation enthalpies depend only on the pressure; (d) steam density and latent heat (H_v) are constant (see Appendix C); (e) steam and water phases are in equilibrium at any time; and (f) axial distribution of the power (or flux) is unchanged during transients.

With these assumptions, Eqs. (10) and (11) give

$$\frac{\partial(A_s U)}{\partial x} + \frac{\partial A_s}{\partial t} = \frac{Q(x,t)}{H_v} - \frac{1}{H_v}\left(\rho_s A_s \frac{dH_s}{dP} + \rho_w A_w \frac{dH_w}{dP}\right) \frac{dP}{dt} \quad . \tag{12}$$

The meaning of the symbols is given in nomenclature.

For small deviations from the steady-state values, Eq. (12) takes the following form:

$$\frac{\partial}{\partial x}(a_s U^0 + u A_s^0) + \frac{\partial a_s}{\partial t} = \frac{q(x,t)}{H_v} - \frac{1}{H_v}\left(\rho_s A_s^0 \frac{dH_s}{dP} + \rho_w A_w^0 \frac{dH_w}{dP}\right) \frac{dP}{dt} \quad , \tag{13}$$

if the second-order terms are ignored.

Equation (13) can be solved for $a_s(x,t)$ when $q(x,t)$ and $P(t)$ are specified, if another relation between $a_s(x,t)$ and $u(x,t)$ can be found. Such a relation can be obtained, at least formally, from the momentum equation.

Instead, the following relation will be postulated in this report for the sake of simplicity of the analysis:

$$A_s^0(x)\,u(x,t) + a_s(x,t)\,U^0(x) \equiv U_p(x)\,a_s(x,t) \quad , \tag{14}$$

where the new function $U_p(x)$ will be called "steam perturbation velocity" for the reason which will be obvious below. The relation between $U_p(x)$ and $U^0(x)$ follows from Eq. (14) as

$$U_p(x) = \gamma(x)\,U^0(x) \quad ,$$

where

$$\gamma(x) = 1 + \frac{A_s^0}{U^0}\,\frac{u(x,t)}{a_s(x,t)} \quad . \tag{15}$$

Equation (15) indicates that the ratio of the relative changes in the steam cross-sectional area and in the steam velocity has been implicitly assumed to be independent of time in the postulated relation, Eq. (14). The physical interpretation of the steam perturbation velocity can be given as follows: A perturbation in the local steam volume causes the steam velocity at that point to change. Therefore, the perturbation propagates with a new steam velocity rather than the unperturbed steady-state steam velocity $U^0(x)$.

The use of Eq. (14) in Eq. (13) yields

$$\frac{\partial(U_p a_s)}{\partial x} + \frac{\partial a_s}{\partial t} = \frac{q(x,t)}{H_v} - \frac{1}{H_v}\left(\rho_s A_s^0\,\frac{dH_s}{dP} + \rho_w A_w^0\,\frac{dH_w}{dP}\right)\frac{dP}{dt} \quad , \tag{16}$$

which will be the fundamental equation of the moderator dynamics in this report.

The validity of the above postulate can be checked by considering the solution of Eq. (16) for a step change in power:

$$a_s(x) = \frac{1}{H_v U_p(x)} \int_0^x q(x')\,dx' \quad .$$

The exact steady-state solution, on the other hand, is found from Eq. (12) as

$$A_s^0(x) = \frac{1}{H_v U^0(x)} \int_0^x Q^0(x')dx' \quad .$$

Since the distribution of the incremental power step q(x) is the same as that of steady-state power $Q^0(x)$, the following relation holds:

$$\frac{a_s(x)}{A_s^0(x)} = \frac{1}{\gamma(x)} \frac{q}{Q^0} \quad , \tag{17}$$

where q and Q^0 are the total powers delivered to the whole channel.

Figures 3, 4 and 5 show the experimental curves representing the variation of the void fraction, i.e., $A_s^0(x)/A$, with position at different power levels and pressures. Designating one power level by Q^0 and the other by $(Q^0 + q)$ in these figures, one obtains the experimental values for A_s^0 and $(A_s^0 + a_s)$. One observes by comparing the experimental values and those predicted from Eq. (17) that the factor $\gamma(x)$ is approximately independent of x. This means that the steady-state steam velocity and the steam perturbation velocity are proportional. The constant value of γ depends on the pressure and on the power level. At atmospheric pressure (Fig. 3), $\gamma = 2$ seems to be an appropriate choice. At higher pressures (Fig. 4), $\gamma = 1$ yields a better agreement. Increasing the power at constant pressure requires higher values of γ (Fig. 5, $\gamma = 2$). The proper value of γ can be obtained in a given application by plotting the void fraction curve at two slightly different power levels.

It is noteworthy to mention that the value $\gamma = 1$ corresponds to the assumption that the steam velocity remains unchanged during the transient. This follows from Eq. (15) by setting $u(x,t) = 0$. Hence, the approximation of constant steam velocity appears to be valid at high pressures as is the case in boiling water power reactors.

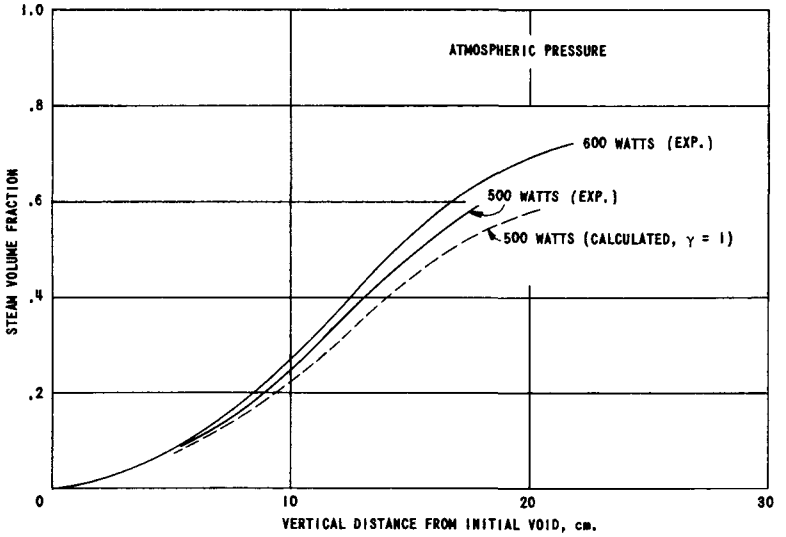

FIG. 3
VOID FRACTION DISTRIBUTION AT ATMOSPHERIC PRESSURE
(EXPERIMENTAL CURVES REPRODUCED FROM FIG. IIA-8 OF REF. 12)

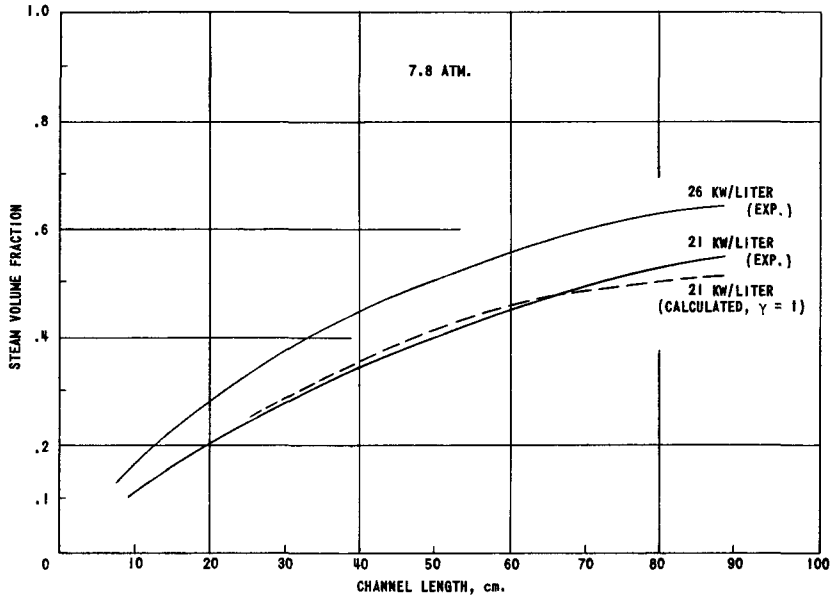

FIG. 4
VOID FRACTION DISTRIBUTION AT 7.8 atm
(EXPERIMENTAL CURVES REPRODUCED FROM FIG. 125 OF REF. 14)

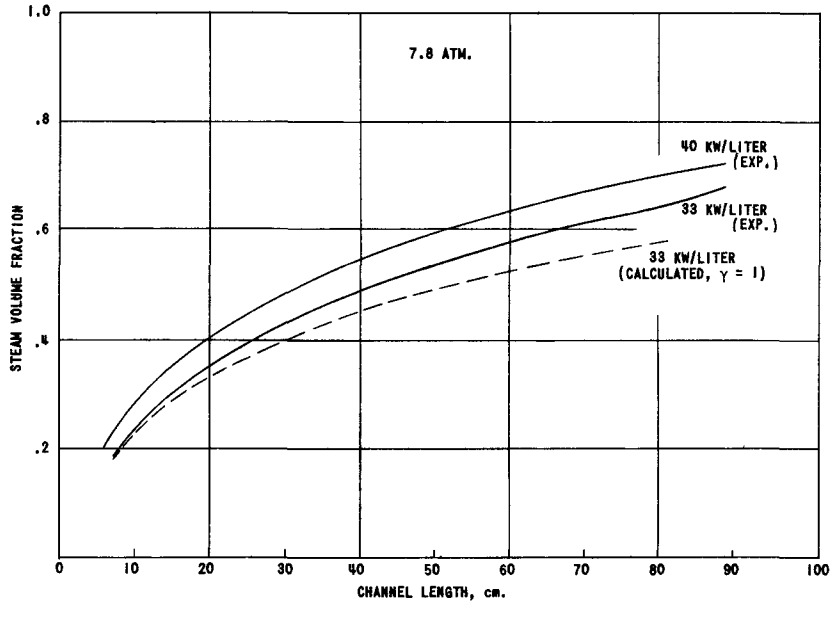

FIG.5
VOID FRACTION DISTRIBUTION AT 7.8 atm
(EXPERIMENTAL CURVES REPRODUCED FROM FIG. 125 OF REF. 14)

In conclusion, one may state that the introduction of the steam perturbation velocity into the theory yields a new adjustable parameter, and thus extends the region of validity of the presented theory.

IV. THE EFFECT OF POWER VARIATIONS

Assume that the heat power delivered into the channel is subjected to small variations while the pressure remains constant. In the boiling region, power variations directly affect the steam production and thus the steam volume. In the nonboiling region, power variations cause the boiling boundary to fluctuate, which in turn gives rise to changes in the steam volume in the boiling region. These two effects will be considered separately.

A. Power-Void Transfer Function

Since the pressure is assumed to remain constant, the last term on the right hand side of Eq. (16) vanishes. Hence, one finds*

$$\frac{\partial(a_s U^0)}{\partial x} + \frac{\partial a_s}{\partial t} = \frac{q(x,t)}{H_v} \quad . \tag{18}$$

The initial and boundary conditions for solving this equation are

$$a_s(x,t) = 0 \qquad \text{for} \qquad t = 0$$

and

$$a_s(x,t) = 0 \qquad \text{for} \qquad x = 0 \quad .$$

The second condition means that there is no change in the position of the boiling boundary with time. The effect of the boiling boundary variations on the steam volume will be treated in Section VII.

In view of the assumption (f) in Section III, viz., $q(x,t)$ has the same spatial distribution as the steady-state flux, one has

$$q(x,t) = \frac{q(t)}{L} D(x) \quad , \tag{19}$$

where $D(x)$ characterizes the steady-state flux distribution and is normalized by means of the expression

$$\frac{1}{L} \int_0^L D(x)\, dx = 1 \quad .$$

---

*No distinction will be made between $U^0(x)$ and $U_p(x)$ in the remaining part of this report, except in Section XIII A, since these velocities are almost identical in high-pressure power reactors.

Combining Eqs. (18) and (19), and using the Laplace transform of $a_s(x,t)$ with respect to t, there is obtained

$$\frac{d[U^0 \overline{a_s}(x,s)]}{dx} + s\,\overline{a_s}(x,s) = \frac{\overline{q}(s)}{L H_v} D(x) \quad . \tag{20}$$

The total variation in the steam volume is obtained by integrating $a_s(x,t)$ along the channel. To calculate the total reactivity change, however, the weighted steam volume has to be considered. The latter is obtained by multiplying the elementary volumes, $a_s(x,t)dx$, by some weighting function F(x). Then, the incremental value of the weighted voids, v(t), is found as

$$v(t) = \int_{L_{nb}}^{L} F(x)\, a_s(x,t)\, dx \quad , \tag{21}$$

where

$$\frac{1}{L} \int_0^L F(x)\ dx = 1 \quad .$$

The Laplace transform of Eq. (21) is

$$\overline{v}(s) = \int_{L_{nb}}^{L} F(x)\, \overline{a_s}(x,s)\, dx \quad . \tag{22}$$

Solving Eq. (20) for $\overline{a_s}(x,s)$ with the boundary condition $\overline{a_s}(L_{nb},s) = 0$ and substituting the solution into Eq. (22) give

$$\frac{\overline{v}(s)}{\overline{q}(s)} = \frac{1}{L H_v} \int_{L_{nb}}^{L} \frac{F(x)}{U^0(x)} dx \int_{L_{nb}}^{x} D(x')\, e^{s[t(x') - t(x)]}\, dx' \quad , \tag{23}$$

where

$$t(x) = \int_{L_{nb}}^{x} \frac{dx'}{U^0(x')} \quad . \tag{24}$$

Equation (23) is the general form of the heat power-void transfer function. The integrations involved in this equation can be performed, at least numerically, if the steady-state flux distribution D(x) and the steam velocity $U^0(x)$ are known.

A factor $e^{-s\tau}$ should be added to the right of Eq. (23) in order to take into account the time delay associated with the formation of steam bubbles in the nucleate boiling. The mechanism of nucleate boiling from a

heating surface was described by Jakob.[8] According to this description, "only a very small amount of the heat produced in the heater is directly transferred to the interior of the bubbles adhering on the surface. The main part of the energy makes a detour through the liquid." The bubbles originate on the roughnesses of the heating surface, and break off when their volume has grown so much that the buoyancy force exceeds the capillary forces which bind them to the heating surface. During the rise of the bubbles in the slightly supersaturated water, the volume of the bubbles continues growing by evaporation through the bubble surface. Steam formation during this period is larger than the initial steam formation on the surface.

Consider an elementary channel section at a given height x where the heat flux undergoes a step change at t = 0. In view of the above explanations, the main part of the heat energy is first transferred to the water, producing a greater degree of supersaturation. The front of the more superheated water will move upwards with the local water velocity. The volume of the steam bubbles coming from the lower sections of the channel will increase, by evaporation through their surface, during the time they travel within the superheated region. As soon as they leave the front of the more saturated region, their sizes will start decreasing as a result of condensation. In this way, the heat energy is transferred to the higher sections of the channel before the water front actually arrives. In other words, the water front will lose its sharpness as it progresses.

One may readily show that a bubble arriving at x at $t = t_1$ will spend a time $[W^0/(U^0-W^0)]t_1$ before it reaches the water front. Suppose that the bubbles acquire their final sizes, which are determined by the superheating available and by the steam flow rate at x, after they spend a time τ_{max} within the supersaturated region. Then, the largest perturbation in the steam fraction in a higher channel section x' will occur after a time

$$\tau(x) = \left(\frac{U^0}{W^0} - 1\right) \tau_{max} \tag{25}$$

following the arrival of the first perturbed bubbles at x' (the change in the steam velocity with perturbation is ignored for the sake of simplicity of this qualitative analysis). The time delay $\tau(x)$ can be interpreted as a delay associated with the steam formation time at x, as long as $(x' - x)$ is larger than $U^0\tau_{max}$ (or τ_{max} is smaller than the steam transit time between the two channel section under consideration). If $(x' - x) < U^0\tau_{max}$, then the maximum perturbation at x' will be experienced after the arrival of the water front. In this case, the time lag will be given by the difference of the water and steam transit times.

One observes that the time delay $\tau(x)$ depends on the channel position insofar as the slip ratio, i.e., $r = (U^0/W^0)$, and τ_{max} are functions of

the position. The latter becomes a function of x because it depends on the bubble concentration at that point. The greater the number of bubbles present, the shorter will τ_{max} be.

One may draw the following qualitative conclusions:

(a) The time delay $\tau(x)$ will be negligible in high-power pressurized boiling water reactors as compared to the steam transit time because the slip ratio approaches unity in such reactors.

(b) Due to the smaller average bubble size in such reactors, τ_{max} also will be small. The dependence of τ_{max} on the bubble size is given by Jakob.[8]

(c) It is noticed that $\tau(x)$ may be appreciable as a consequence of a large slip ratio, even if τ_{max} is small.

(d) An average delay (τ) may be defined for the whole channel to take into account the effect of the distributed time delay associated with the steam formation, viz., $\tau(x)$, in a lumped manner. It is this averaged delay time which would give rise to an exponential factor, $\exp(-s\tau)$, in Eq. (23), as previously mentioned. This factor will not be considered in the following analysis, since we will be mainly concerned with the high-power pressurized boiling water reactors.

A specific expression for the power-void transfer function given in Eq. (24) will now be obtained in the case of a uniform steam velocity and a sinusoidal flux distribution, i.e.,

$$U^0(x) = U_0$$

and

$$D(x) = \frac{\pi}{2} \sin \pi \frac{x}{L} \quad , \tag{26}$$

where U_0 is the average steam velocity in the boiling region. The actual flux distribution can be better approximated by a sinusoidal curve if L in Eq. (26) is interpreted as a properly reduced core height instead of the actual core height (see Fig. 6). By doing this, one takes into account the flux depression near the top of the core due to the voids.

When evaluating the zero-frequency response, the variation of the steam velocity along the channel can be taken into account without much complexity. Assume that

$$U^0(x) = U_1 e^{bx} \quad ,$$

where U_1 is the steam velocity at the boiling boundary, and b is a parameter related to the outlet steam velocity U_2 as $b = (1/L_b') \ln(U_2/U_1)$. The choice

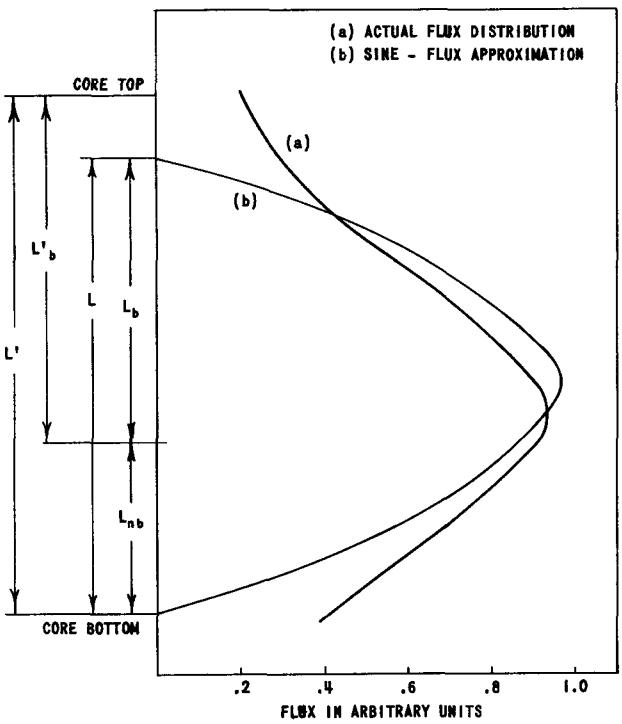

FIG. 6
AXIAL FLUX DISTRIBUTION IN EBWR AT 20 Mw AND 41 atm

of an exponential distribution, to take into account the variation of the steam velocity, is mainly a matter of mathematical convenience. Other forms, such as a linear or a quadratic distribution, require more involved calculations. Moreover, theoretical considerations qualitatively indicate that the increase of the steam velocity in the boiling region may be more rapid than a linear rise. Therefore, the exponential distribution seems to be reasonable.

The weighting function F(x) will be assumed to be identical with D(x). This assumption corresponds to the first-power flux weighting, as explained in the introduction.

With these assumptions, zero-frequency response is obtained from Eq. (23) as

$$\frac{\bar{v}(0)}{\bar{q}(0)} = \frac{\pi^2}{4LH_v U_1}\left\{\frac{\cos\alpha}{b^2+(\pi/L)^2}\left(\cos\alpha - \frac{bL}{\pi}\sin\alpha - e^{-bL_b}\right)\right.$$

$$\left. + \frac{1}{b^2+(2\pi/L)^2}\left(e^{-bL_b} + \frac{bL}{2\pi}\sin 2\alpha - \cos 2\alpha\right)\right\} \quad , \qquad (27)$$

where

$$\alpha = (\pi L_b/L) \quad .$$

For the calculations of Eq(23) as a function of frequency, a uniform steam velocity will be assumed to avoid unjustifiably tedious manipulations. Then, Eq. (23) yields

$$\frac{\bar{v}(z)}{\bar{q}(z)} = \frac{\pi}{4H_v\omega_s}\frac{1}{1+z^2}\left\{\frac{z}{4}(2\alpha - \sin 2\alpha) - \frac{1-\cos 2\alpha}{4}\right.$$

$$\left. + \frac{1}{1+z^2}\left[1 - e^{-z\alpha}(z\sin\alpha + \cos\alpha)\right]\right\} \quad , \qquad (28)$$

where

$$z = s/\omega_s$$
$$\alpha = \pi L_b/L$$
$$\omega_s = \alpha/T_s$$
$$T_s = L_b/U_0 \quad .$$

Zero-frequency response in the case of uniform steam velocity is obtained from Eq. (28) by setting z = 0 or from Eq. (26) by setting b = 0 and $U_1 = U_0$:

$$\frac{\bar{v}(0)}{\bar{q}(0)} = \frac{\pi(1 - \cos\alpha)^2}{8H_v\omega_s} \quad .$$

High-frequency response of Eq. (28) approaches

$$\frac{\bar{v}(z)}{\bar{q}(z)} = \frac{\pi(2\alpha - \sin 2\alpha)}{16\,H_v\omega_s}\,\frac{1}{z} \quad , \qquad \text{for} \quad |z| > 1 \quad .$$

The fact that the high-frequency response falls 6 db per octave suggests that the transfer function in Eq. (28) can be approximated by a single time constant, i.e.,

$$\frac{\bar{v}(s)}{\bar{q}(s)} = \frac{\pi(1 - \cos\alpha)^2}{8\,H_v\omega_s}\,\frac{1}{1 + s\tau_{qv}} \quad , \tag{29}$$

where

$$\tau_{qv} = \frac{2(1 - \cos\alpha)^2}{(2\alpha - \sin 2\alpha)\alpha}\,T_s \quad . \tag{30}$$

This simplified transfer function approaches the exact one at low and high frequencies, both in magnitude and phase. However, some discrepancies may occur in the intermediate frequency range about ω_s.

Note that the gain of Eq. (29) vanishes when $\alpha = 0$, i.e., when there is no boiling in the core, as one would expect.

Note also that the cofactor of T_s in Eq. (30) is not sensitive to the values of α, i.e., to the position of the boiling boundary (0.375 for $\alpha = 0$, 0.40 for $\alpha = \pi$). For the average boiling height in EBWR, $\alpha = 2\pi/3$ and $\tau_{qv} = 0.42\ T_s$.

In Fig. 7, the amplitude of the exact and simplified transfer functions, namely Eqs. (28) and (29), are plotted. It is observed that the discrepancy in the intermediate range is appreciable in the case of $\alpha = \pi$ and $\alpha = 2\pi/3$. One may desire to have a better fit in this frequency region at the expense of the

high-frequency fitting, since the resonance peak of the overall transfer function usually occurs in this region. Figure 8 shows that this correction can be made by decreasing τ_{qv} by a factor of approximately 0.80. For smaller values of α, such as $\pi/3$, no correction is needed. For EBWR, the corrected time constant becomes

$$\tau_{qv} = T_s/3 \quad .$$

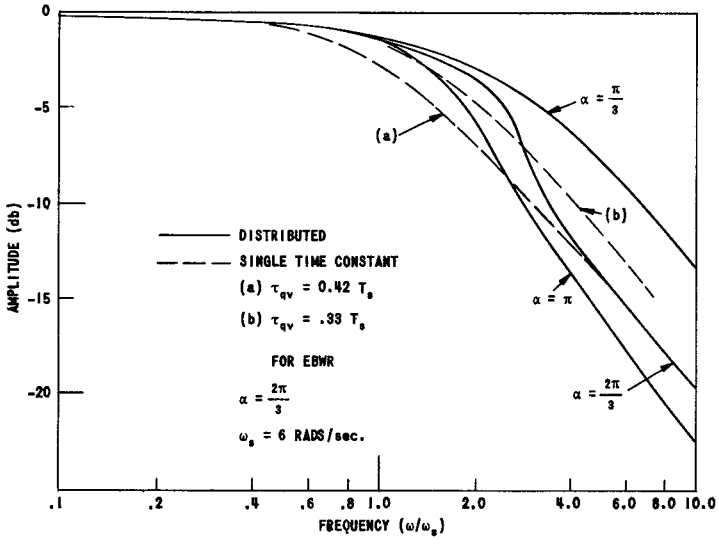

FIG. 7
AMPLITUDE RESPONSE OF POWER-VOID TRANSFER FUNCTION

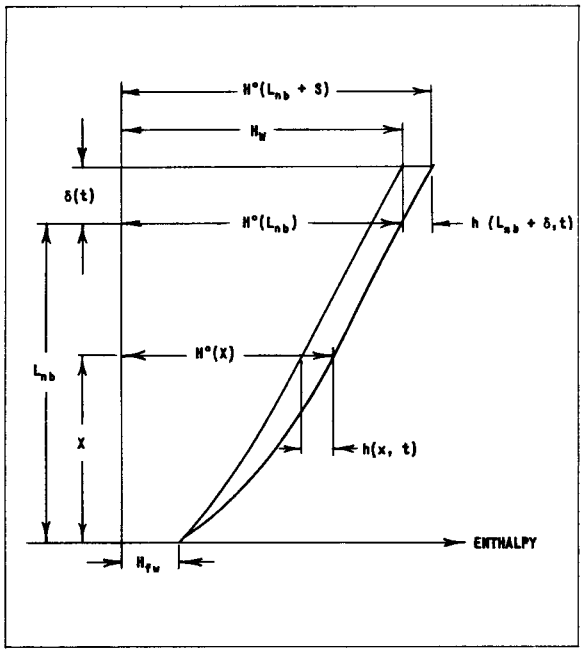

FIG. 8
BOUNDARY SHIFT DUE TO STEP POWER CHANGE

B. Power-Boiling Boundary Transfer Function

The effect of the power variations on the boiling boundary will now be considered. The transfer function associated with the heat transfer in the nonboiling region is obviously similar to that in the boiling region. The only difference lies in the value of the thermal resistance R_3.

The heat supplied to the channel in the nonboiling region brings the subcooled water to the saturation temperature at the boiling boundary. Assuming that the recirculation water entering the core is at saturation temperature, the variation of the feedwater enthalpy along the channel is given by

$$\dot{M}_{fw} \frac{dH^0(x)}{dx} = Q^0(x) \quad , \tag{31}$$

which is obtained from Eq. (11) by setting $A_s = 0$ (no steam) and $\dot{M}_{fw} = \rho_w A W_0^0$. Boiling starts at $x = L_{nb}$, where $H^0(L_{nb}) = H_w$. Hence, the boiling height is determined as

$$\dot{M}_{fw} (H_w - H_{fw}) = \int_0^{L_{nb}} Q^0(x)\, dx \quad . \tag{32}$$

With the incremental values, Eq. (11) yields the following equation in the nonboiling region:

$$\frac{\partial h(x,t)}{\partial x} + \frac{1}{W_0^0} \frac{\partial h(x,t)}{\partial t} = \frac{q(x,t)}{\dot{M}_{fw}} \quad . \tag{33}$$

Initial and boundary conditions are: $h(x,0) = 0$ and $h(0,t) = 0$. The latter implies that the enthalpy of the coolant at the inlet is constant. The variations of the coolant enthalpy, such as those caused by pressure variations, will be separately treated in a later section.

The solution of Eq. (33) is straightforward:

$$\dot{M}_{fw} \bar{h}(x,s) = \frac{\bar{q}(s)}{L} \int_0^x D(x')\, e^{-\frac{s}{W_0^0}(x - x')}\, dx' \quad . \tag{34}$$

Inspection of Fig. 8 reveals that the following relation holds at the boiling boundary at any time:

$$H^0(L_{nb} + \delta) + h(L_{nb} + \delta, t) = H_w \quad . \tag{35a}$$

Since the variation of h is a second-order quantity when x increases from L_{nb} to $(L_{nb} + \delta)$, it is seen that $h(L_{nb} + \delta, t)$ may be replaced by $h(L_{nb}, t)$. On the other hand, Eq. (31) yields

$$H^0(L_{nb} + \delta) - H^0(L_{nb}) = \frac{Q^0(L_{nb})}{\dot{M}_{fw}} \delta(t) \quad . \tag{35b}$$

Then, one obtains from Eqs. (35a) and (35b) that

$$\delta(t) = -\frac{1}{Q^0(L_{nb})} \dot{M}_{fw} h(L_{nb}, t) \tag{36}$$

or, by combining the Laplace transform of Eq. (36) with Eq. (34),

$$\frac{\overline{\delta}(s)}{\overline{q}(s)} = -\frac{1}{LQ^0(L_{nb})} \int_0^{L_{nb}} D(x') e^{-s(L_{nb}-x')/W} dx' \quad . \tag{37}$$

Equation (37) is the general form of the power-boiling boundary transfer function.

In the case of sinusoidal flux distribution, Eq. (37) becomes

$$\frac{\overline{\delta}(z)}{\overline{q}(z)} = -\frac{1}{2Q^0(L_{nb})} \frac{e^{-\beta z} + z \sin\beta - \cos\beta}{1 + z^2} \tag{38}$$

where

$$z = s/\omega_w$$
$$\omega_w = \beta/T_w$$
$$\beta = \pi L_{nb}/L$$
$$T_w = L_{nb}/W_0^0 \quad .$$

The single-time-constant approximation is obtained from Eq. (38) by matching the high-frequency and the zero-frequency responses. The last factor in Eq. (38) reduces to $(1 - \cos\beta)$ at low frequencies and approaches $(\sin\beta)/z$ at sufficiently high frequencies, where $|z \sin\beta| >> (1 - \cos\beta)$ holds. Hence,

$$\frac{\overline{\delta}(s)}{\overline{q}(s)} = -\frac{1 - \cos\beta}{2Q^0(L_{nb})} \frac{1}{1 + s\tau_{qb}} \quad , \tag{39}$$

where

$$\tau_{qb} = \frac{1 - \cos\beta}{\beta \sin\beta} T_w \quad .$$

In Fig. 9, the exact and simplified transfer functions are compared by plotting their amplitudes vs the frequency. Two values of β, namely, $\beta = \pi/3$ and $\beta = \pi$, are considered. The former value corresponds to the nonboiling length in EBWR, whereas the latter corresponds to the case in which boiling starts just at the top of the core.

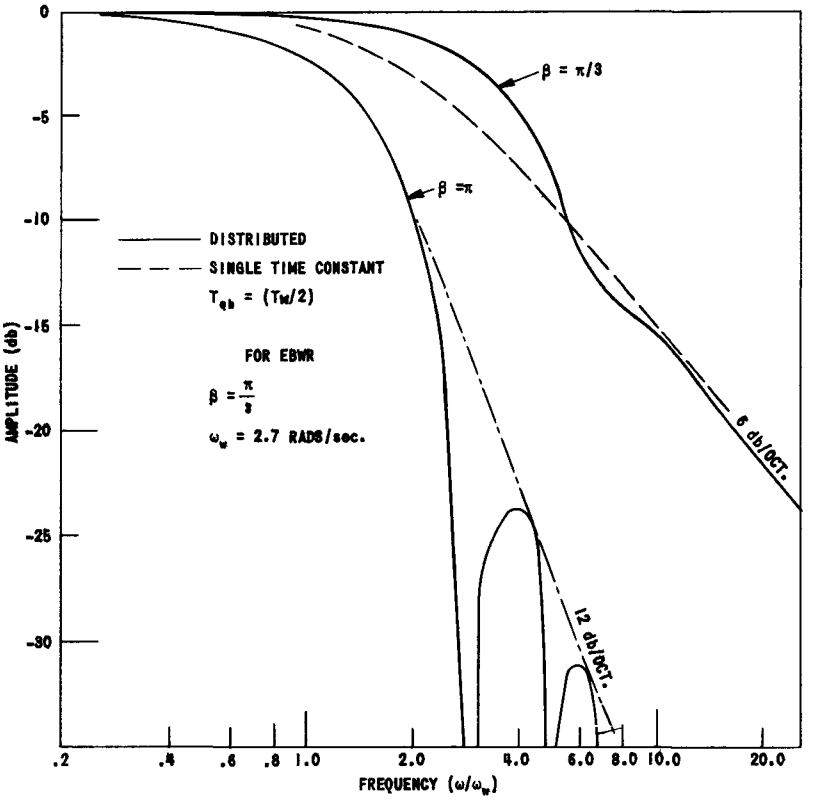

FIG. 9
AMPLITUDE RESPONSE OF POWER-BOILING BOUNDARY TRANSFER FUNCTION

It is observed that the single-time-constant approximation fails to be satisfactory when $\beta = \pi$. In this extreme case, the amplitude of the transfer function vanishes at frequencies which are odd integral multiples of (π/T_w) rad/sec. This resonance phenomenon would not be observed in an actual reactor since it is extremely unlikely that the amplitude would vanish at the same frequency in each channel of the core. Therefore, one may take the envelope of the peaks as the overall transfer function of the reactor. Since the envelope falls 12 db per octave at high frequencies, at least two time constants are necessary for a reasonable fit when the boiling starts near the top of the core.

A physical insight into this resonance phenomenon can be obtained by considering the simpler model where the heat production is uniform. Substitution of D(x) = 1 in Eq. (37) yields

$$\frac{\bar{\delta}(s)}{\bar{q}(s)} = -\frac{L_{nb}}{L}\frac{1}{Q^0(L_{nb})}\frac{1 - e^{-sT_w}}{sT_w} \quad . \tag{40}$$

The behavior of this transfer function is investigated in Appendix A. It is shown there that the amplitude vanishes, in this case, at the integral multiples of $2\pi/T_w$ regardless of the position of the boiling boundary (in the case of sinusoidal heat production, the resonance occurs only when the boiling boundary is near the top of the core).

At the resonance frequency, water particles experience a complete cycle of the power variation during their transit time in the nonboiling region. Therefore, the net change in the water enthalpy amounts to zero at the boiling boundary, and thus no change occurs in the position of the boiling boundary.

The single-time-constant approximation is obtained, in the case of uniform heat generation, by considering the envelope of the peaks (see Appendix A) rather than by matching the high and low-frequency responses. The time constant turns out to be $T_w/2$ for any value of β. A comparison of this time constant with τ_{qb} in Eq. (39) shows that the latter approaches $T_w/2$ for small values of β. For large values of β, it tends to infinity, confirming that the single-time-constant approximation is no more valid for these values of β. One concludes from these considerations that the time constant $T_w/2$ is the best choice for any value of β, if the single-time-constant approximation is preferred for the sake of simplicity.

V. THE EFFECTS OF PRESSURE VARIATIONS

Two effects of the pressure variations will be considered in this section. The first one is the immediate effect on the steam volume in the boiling region due to the steam condensation or water flashing. The second effect is on the boiling boundary position as a consequence of the saturation temperature change due to the pressure.

A. Pressure Rate-Steam Void Transfer Function

It is assumed that the condensation, as well as flashing, takes place instantaneously after a pressure change, so that both the steam and water remain saturated at any time. In view of this assumption, one is allowed to use Eq. (16), which gives

$$\frac{\partial(a_s U^0)}{\partial x} + \frac{\partial a_s}{\partial t} = K(x) \frac{dP}{dt} \quad , \tag{41}$$

where

$$K(x) = -\frac{1}{H_v} \left(\rho_s A_s^0 \frac{dH_s}{dP} + \rho_w A_w^0 \frac{dH_w}{dP} \right) . \tag{42}$$

In Eq. (42), dH_s/dP and dH_w/dP are evaluated at the steady-state pressure.

Initial and boundary conditions for Eq. (41) are $a_s(x,0) = 0$ and $a_s(0,t) = 0$. The second condition implies that the boiling boundary remains unchanged. The effect of the boiling boundary variations on the steam volume will be treated in Section VII.

Using the procedure followed in solving Eq. (18), one obtains the solution of Eq. (41) as

$$\frac{\bar{v}(s)}{s\bar{p}(s)} = \int_{L_{nb}}^{L} \frac{F(x)}{U^0(x)} dx \int_{L_{nb}}^{x} K(x') \, e^{s[t(x') - t(x)]} \, dx' , \tag{43}$$

where $t(x)$ is given by Eq. (24). This equation gives the pressure rate-void transfer function.

To determine the explicit form of $K(x)$, one has to know $A_s^0(x)$ and $A_w^0(x)$. Since $A = A_s^0 + A_w^0$, it suffices to determine $A_s^0(x)$ only. The latter is the steady-state solution of Eq. (12):

$$A_s^0(x) = \frac{Q^0}{LH_v U^0(x)} \int_{L_{nb}}^{x} D(x') \, dx' \quad . \tag{44}$$

Combination of Eqs. (42) and (44) gives the explicit form of K(x) as

$$K(x) = -\frac{A\rho_w(dH_w/dP)}{H_v}\left[1+\frac{Q^0}{LH_vA(dH_w/dP)U^0(x)}\left(\frac{dH_s}{dP}\frac{\rho_s}{\rho_w}-\frac{dH_w}{dP}\right)\int_{L_{nb}}^{x} D(x')\,dx'\right] . \tag{45}$$

Comparison of Eqs. (18) and 41) indicates that the transient behavior of the total void volume after a step change in pressure is different from that following a step change in power, in spite of the fact that both transients end at the same time. The difference comes from the fact that the right side of Eq. (41) contains in K(x) the integrated power, whereas the right side of Eq. (18) contains the differential power.

In the case of uniform steam velocity, sinusoidal flux distribution, and first-power flux weighting, Eq. (43) becomes

$$\frac{\bar{v}(s)}{s\bar{p}(s)} = K_1\frac{1-\cos\alpha}{z} - \frac{e^{-\alpha z}+z\sin\alpha-\cos\alpha}{1+z^2}\left(K_2\frac{\sin\alpha - z\cos\alpha}{1+z^2}+\frac{K_1}{z}\right)$$

$$+\frac{K_2}{4}\frac{1}{1+z^2}(2\alpha-\sin 2\alpha-2z\sin^2\alpha) , \tag{46}$$

where

$$K_1 = \frac{AL}{2H_v\omega_s}\left[\left(\rho_w\frac{dH_w}{dP}-\rho_s\frac{dH_s}{dP}\right)\frac{Q^0\cos\alpha}{2U_0AH_v}-\rho_w\frac{dH_w}{dP}\right] \tag{47}$$

and

$$K_2 = -\frac{Q^0L}{4U_0H_v^2\omega_s}\left(\rho_w\frac{dH_w}{dP}-\rho_s\frac{dH_s}{dP}\right) . \tag{48}$$

The single-time-constant approximation is obtained by considering the zero and high-frequency responses as

$$\frac{\bar{v}(s)}{s\bar{p}(s)} = \frac{C_0}{1+s\tau_{pv}} , \tag{49}$$

where

$$C_0 = (K_2/4)(2\alpha - 4\sin\alpha+\sin 2\alpha)+K_1(\alpha-\sin\alpha)$$

and

$$\tau_{pv} = \frac{2C_0}{\alpha[2K_1(1-\cos\alpha)-K_2\sin^2\alpha]}T_s . \tag{50}$$

It is interesting to note that both the gain and the time constant of the pressure rate-void transfer function increase with power. This is the only feedback mechanism whose time constant is dependent upon power. The physical interpretation of this dependence follows explicitly from the fact that the initial excess steam distribution, after a step pressure change, is approximately the same as the steady-state water mass distribution. At higher powers, the water mass decreases more rapidly towards the top of the channel. Therefore, an increase in power will result in more initial excess steam near the center and thus in larger time constants.

It has to be noted also that the pressure rate-void feedback is a positive feedback, as one can visualize physically. This fact is implied in the sign of C_0, which is found to be negative when numerical values are introduced.

Derivation of the pressure rate-void transfer function is based on the assumption that water is always present in the boiling channel. Therefore, it would not be valid at high power levels for which the above condition is not satisfied (complete boiling, i.e., $A_S^0(L) = A$).

Figure 10 shows the amplitude responses of EBWR (for 20 Mw at 41 atm) in terms of Eqs. (46) and (49). The single-time-constant approximation proves to be quite satisfactory for all frequencies.

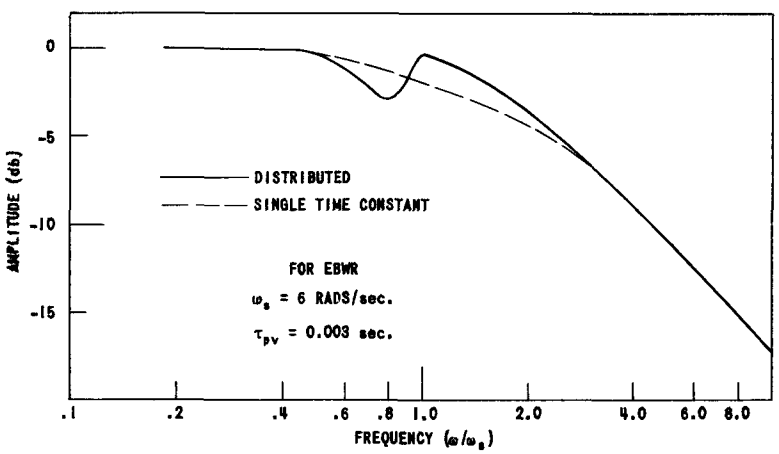

FIG. 10
AMPLITUDE RESPONSE OF PRESSURE-VOID TRANSFER FUNCTION

B. Pressure-Boiling Boundary Transfer Function

The position of the boiling boundary fluctuates with pressure as a consequence of the changes in the saturation enthalpy of water. The relation between the water enthalpy and the boiling height variation can be obtained from Eq. (32) as

$$\dot{M}_{fw}\,(H_w + h_w - H_{fw}) + \dot{M}_r\,h_w = \int_0^{L_{nb}+\delta} Q^0(x)\,dx \qquad (51)$$

if the enthalpy change in the recirculating water is taken into account. Substraction of Eq. (32) from Eq. (51) gives

$$\delta = \frac{\dot{M}_t}{Q^0(L_{nb})}\,h_w \quad , \qquad (52)$$

where

$$\dot{M}_t = \dot{M}_{fw} + \dot{M}_r .$$

The transient involved in this phenomenon lasts until the arrival of the recirculating water at the new saturation temperature. If $\dot{M}_r >> \dot{M}_{fw}$, one may show[1] that the boundary returns to its original position after the recirculation time T_r, following a step pressure change. Therefore, the pressure-boiling boundary transfer function follows from Eq. (52) as

$$\frac{\bar{\delta}(s)}{s\bar{p}(s)} = \frac{dH_w}{dP}\,\frac{\dot{M}_t}{Q^0(L_{nb})}\,\frac{1 - e^{-sT_r}}{s} \quad . \qquad (53)$$

The definition of the recirculation time needs further attention. It should be defined, for each stream filament in the downcomer, as the water transit time between the saturated region in the vessel and the boiling boundary. Hence, the value of the recirculation time is different in each filament because of the difference in their length and velocity. The spread in T_r can be taken into account by defining an average transfer function, as explained in Appendix A. Use of the results of Appendix A in Eq. (53) yields

$$\frac{\bar{\delta}(s)}{s\bar{p}(s)} = \frac{dH_w}{dP}\,\frac{\dot{M}_t}{Q^0(L_{nb})}\,\frac{T_r}{1 + sT_r} \quad , \qquad (54)$$

where T_r denotes the averaged recirculation time. Equation (54) is the pressure rate-boiling boundary transfer function.

VI. THE EFFECT OF THE FEEDWATER FLOW VARIATIONS

The position of the boiling boundary is also affected by the variations in the feedwater flow. By differentiation, one obtains from Eq. (32)

$$\dot{m}_{fw}\,(H_w - H_{fw}) = Q^0(L_{nb}) \quad .$$

The feedwater-boiling boundary transfer function is then found as

$$\frac{\bar{\delta}(s)}{\bar{\dot{m}}_{fw}(s)} = \frac{H_w - H_{fw}}{Q^0(L_{nb})}\, e^{-sT_r'} \quad , \tag{55}$$

where the exponential factor accounts for the finite recirculation time T_r' between the inlet of the feed water and the boiling boundary.

VII. BOILING BOUNDARY-VOID TRANSFER FUNCTION

Variation of the boiling boundary will cause the total steam volume in the channel to fluctuate, since a change in the boiling height can be regarded as a change in the steam production at the boiling boundary, and thus as an additional lumped steam source.

If δ denotes the shift of the boundary, the strength of this fictitious source can be given as $\delta\, Q^0(L_{nb})/H_v$. The perturbation in the steam volume, after a step change in the boiling height, will move upwards as a step wave front. Steady state at each point will be reached once the wave front arrives at that point.

The following equation is readily obtained from the steam-mass continuity at a level x, where the steady state has already been reached:

$$U^0(x)\, a_s(x) = -\frac{Q^0(L_{nb})}{H_v}\, \delta \quad . \tag{56}$$

The minus sign indicates that an increase in nonboiling length results in a decrease in steam volume.

The transient in the core ends when the wave front reaches the top of the channel, viz., at $t = T_s$. The total change in the weighted steam volume at a time t during the transient is obtained as

$$v(t) = \int_{L_{nb}}^{x(t)} a_s(x')F(x')\, dx' \quad , \tag{57}$$

for $t \leqq T_s$, where x(t) denotes the position of the wave front at the time t.

The relation between x and t is given by

$$t = \int_{L_{nb}}^{x(t)} \frac{dx'}{U^0(x')} \quad . \tag{58}$$

After the steady state has been reached, i.e., $t \geq T_s$, v(t) remains constant:

$$v(t) = \int_{L_{nb}}^{L} a_s(x')F(x')\, dx' \quad , \tag{59}$$

for $t \geq T_s$.

Combination of Eqs. (56), (57), (58) and (59) and the use of the Laplace transforms yield

$$\frac{\bar{v}(s)}{\bar{\delta}(s)} = -\frac{Q^0(L_{nb})}{H_v} \int_0^{T_s} F[x(t)]\, e^{-st}\, dt \quad , \tag{60}$$

which is the general form of the boiling boundary-void transfer function.

The zero-frequency response of Eq. (60) for a sinusoidal flux weighting and an exponential steam velocity distribution is found as

$$\frac{\bar{v}(0)}{\bar{\delta}(0)} = -\frac{Q^0(L_{nb})}{H_v}\left[\frac{\pi^2}{2U_1L}\,\frac{1}{b^2+(\pi/L)^2}\left(e^{-bL_b} + \frac{bL}{\pi}\sin\alpha - \cos\alpha\right)\right] . \tag{61}$$

In the special case of no weighting, viz., F(x) = 1, Eq. (60) gives

$$\frac{\bar{v}(s)}{\bar{\delta}(s)} = -\frac{Q^0(L_{nb})}{H_v}\,\frac{1-e^{-sT_s}}{s} \quad . \tag{62}$$

When sinusoidal weighting and the constant-steam velocity approximation are used, Eq. (60) yields

$$\frac{\bar{v}(s)}{\bar{\delta}(s)} = -\frac{Q^0(L_{nb})}{H_v}\,\frac{\pi}{2}\,\frac{e^{-\alpha z} + z\sin\alpha - \cos\alpha}{\omega_s(1+z^2)} \quad . \tag{63}$$

It is recognized that the forms of Eqs. (62) and (63) are the same as those of Eqs. (40) and (38), respectively. Following the same procedure used in treating the latter equations, there is obtained

$$\frac{\overline{v}(s)}{\overline{\delta}(s)} = -\frac{Q^0(L_{nb})}{H_v}\,\frac{\pi}{2}\,\frac{1-\cos\alpha}{\alpha}\,\frac{T_s}{1+s(T_s/2)}\quad , \tag{64}$$

which is the approximated boiling boundary-void transfer function.

Figure 11 displays a comparison of the exact and the approximated transfer functions for $\alpha = 2\pi/3$, which is the case for EBWR. One observes that the single-time-constant approximation is not satisfactory in the intermediate frequency region. More than one time constant is necessary for a better approximation.

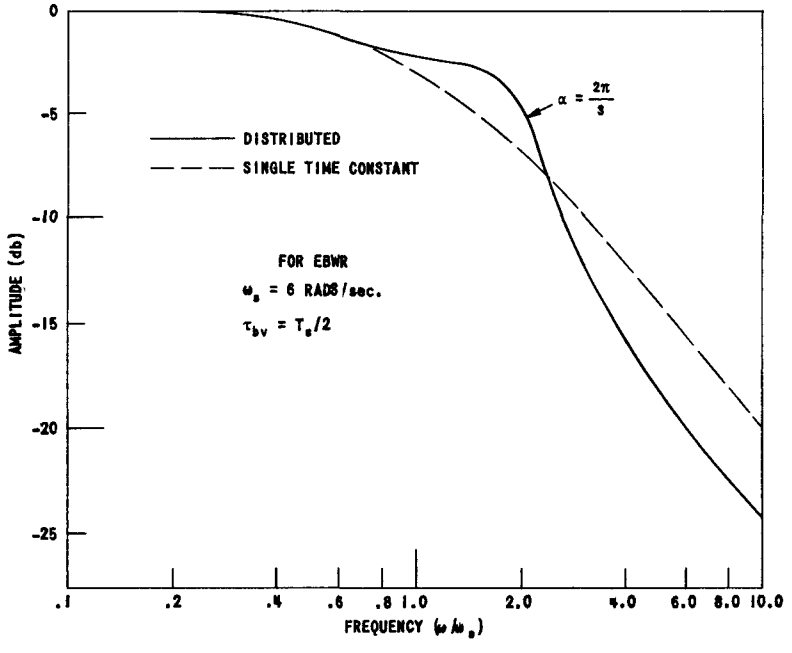

FIG. 11
AMPLITUDE RESPONSE OF BOILING BOUNDARY-VOID TRANSFER FUNCTION

The resonance phenomenon described in Section IV B will also occur in the boiling region when α approaches π, i.e., when the boiling starts near the bottom of the core. In the latter case, the amplitude of Eq. (63) vanishes at the odd integral multiples of (π/T_s) rad/sec.

Physical interpretation becomes more evident if the case of non-weighting is considered. As one observes from Eq. (62), resonance occurs, in this simpler case, at integral multiples of $(2\pi/T_s)$, i.e., when the transit time is equal to the integral multiples of the period of the sinusoidal boundary variations. At resonance, the boiling length contains one or more complete cycles, and therefore the integrated steam volume amounts to zero at any time.

Note also that the resonance occurs for any boiling height, in contrast to the sinusoidal weighting model. The effect of the weighting on the resonance frequency is also worth mentioning: the first resonance appears at a lower frequency due to the weighting.

VIII. THE EFFECT OF WATER ACCELERATION

In the previous sections water velocity in the nonboiling region and in the downcomer was assumed to remain constant during the transients. In fact, any transient of the steam volume in the core is accompanied by a change in the water velocity, as a consequence of the change in the pressure head. The effect of the water acceleration is such that it tends to smooth the steam-void variations within the core, causing the steam to pass more rapidly through the core when there is an increase in the steam volume, or vice versa. The purpose of this section is to calculate the net void volume in the presence of the water acceleration.

The analysis starts with the momentum equation in the recirculating loop:

$$\frac{d\Sigma}{dt} = \Delta P - P_i - P_f \quad , \tag{65}$$

where Σ is the total momentum in the circulation loop, ΔP is the driving force, and P_i and P_f are the inertial and frictional forces. Explicit forms of these quantities are as follows:

$$\Sigma = \int_{x_1}^{x_3} (\rho_s A_s U + \rho_w A_w W)dx + \left(M_{nb} + \frac{A}{A_d} M_d\right) W_0 + \rho_w L_s \frac{dV}{dt} \quad , \tag{66}$$

$$\Delta P = g \int_{x_1}^{x_3} (\rho_w - \rho_s) A_s \, dx \quad , \tag{67}$$

$$P_i = [\rho_s U^2(x_3,t) A_s(x_3,t) + \rho_w W^2(x_3,t) A_w(x_3,t)] - \rho_w A W_0^2 \tag{68}$$

$$P_f = C_1 W_0^2 + C_2 \int_{x_1}^{x_3} W^2(x,t) \, dx \quad , \tag{69}$$

where the meanings of the symbols are given either in the nomenclature or in Fig. 12. The first integral term in Eq. (66) is the momentum in the boiling region. The second term is the momentum of the water in the nonboiling region and in the downcomer. The ratio A/A_d takes into account

the difference between the downcomer and the core inlet velocities. The last term accounts for the momentum of the water above the core during the transients.[9]

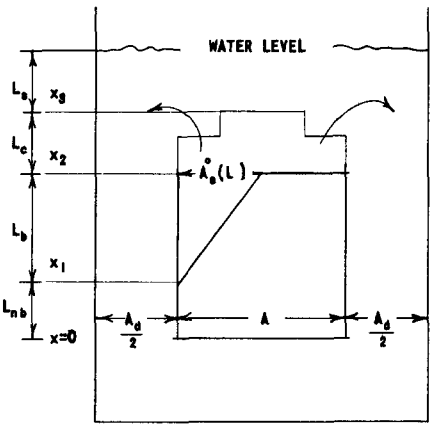

FIG. 12
SCHEMATIC DIAGRAM OF RECIRCULATION LOOP

At steady state, Eq. (65) reduces to

$$\Delta P^0 = P_i^0 + P_f^0 \quad .$$

One may define an overall friction coefficient B relative to the water velocity in the steady state as[10]

$$\Delta P^0 = B\, W_0^{0\,2} \quad .$$

Assuming that B is constant during transients of sufficiently small amplitude, one may replace the last two terms in Eq. (65) by $2BW_0^0 w_0$, where w_0 denotes the incremental value of the water velocity at the core inlet.

The incremental value of the momentum in Eq. (66) may be approximately given as $M' w_0$, where

$$M' = M_b + M_{nb} + M_d(A/A_d) \quad . \tag{70}$$

In this approximation, the integral in Eq. (66) is replaced by $M_b w_0$, assuming that the distributions of the steam and water velocities and of the steam cross section do not change during the transient. Only the translational velocity of the whole two-phase system increases by the amount of w_0.

The last term in Eq. (66) contains the time derivative of the total incremental void volume in the core as well as in the chimney. For slow transients, the variation of this term may be neglected. Then Eq. (65)

reduces, in incremental values, to

$$M' \frac{dw_0}{dt} + 2BW_0^0 w_0 = g(\rho_w - \rho_s) \int_{x_1}^{x_3} a_s(x,t)\, dx \quad . \tag{71}$$

It is now assumed that $a_s(x,t)$ is distributed in the active core with the steady-state steam distribution for all values of t. This assumption is justified as follows: Consider a step change in one or more reactor parameter at $t = 0$. The excess steam, produced by this perturbation in the core, will reach the steady-state steam distribution after the core steam transit time T_s. At this instant, the steam flow into the chimney attains its maximum and remains so thereafter. Therefore, by ignoring the total steam volume change in the core and in the chimney prior to $t = T_s$, one may visualize a step change in the steam volume of the core at the time $t = T_s$ with the steady-state distribution. Then, a step wave front with a constant amplitude starts moving upwards with the outlet steam velocity, immediately after the change in the core steam volume is experienced. The amplitude of this progressive wave is given as $2v_n/L_b$ if the steady-state steam distribution is assumed to be linear (v_n denotes the net steam volume change in the core).

With these considerations, the incremental momentum equation, viz., Eq. (65), can be written as (measuring x from the top of the core)

$$M' \frac{dw_0}{dt} + 2BW_0^0 w_0 = g(\rho_w - \rho_s) \left\{ v_n(t) + \frac{2}{L_b} \int_0^{L_c} v_n \left(t - [x/U^0(L_b)]\right) dx \right\} \quad . \tag{72}$$

Using the Laplace transforms and the standard technique of approximation of the previous chapters, there is obtained

$$\frac{\bar{w}_0(s)}{\bar{v}_n(s)} = \frac{g\rho_w}{2BW_0^0} \left(1 + \frac{2L_c}{L_b}\right) \frac{1 + sT_2}{(1 + sT_1)[1 + (sT_c/2)]} \quad , \tag{73}$$

where

$$T_c = L_c/U^0(L_b) \quad \text{(Chimney transit time)}$$

$$T_1 = M'/2BW_0^0$$

$$T_2 = \frac{T_c/2}{1 + 2(L_c/L_b)} \quad .$$

The desired transfer function $\bar{v}_n(s)/\bar{v}(s)$ is obtained from the diagram shown in Fig. 13:

$$\frac{\bar{v}_n(s)}{\bar{v}(s)} = G\,\frac{(1+sT_1)\left(1+s\,\frac{T_c}{2}\right)}{1+s\eta+s^2\,\zeta} \quad , \tag{74}$$

where

$$\frac{1}{G} = 1 - \frac{g\rho_w}{2BW_0^0}\left(1+\frac{2L_c}{L_b}\right)\frac{\partial V}{\partial W_0}$$

$$\eta = G\left[T_1 + \frac{T_c}{2}\left(1 - \frac{g\rho_w}{2BW_0^0}\,\frac{\partial V}{\partial W_0}\right)\right]$$

and

$$\zeta = GT_1T_c/2 \quad .$$

The value of $\partial V/\partial W_0$ can be evaluated from

$$V = A\int_{L_{nb}}^{L} \frac{\int_{L_{nb}}^{x} Q^0(x')\,dx'}{rW_0H_vA + \int_{L_{nb}}^{x} Q^0(x')\,dx'}\,dx \quad ,$$

which follows from the continuity equation, viz., Eq. (12), in the steady state, assuming that the slip ratio r is constant and ignoring $r\rho_s$ compared to ρ_w.

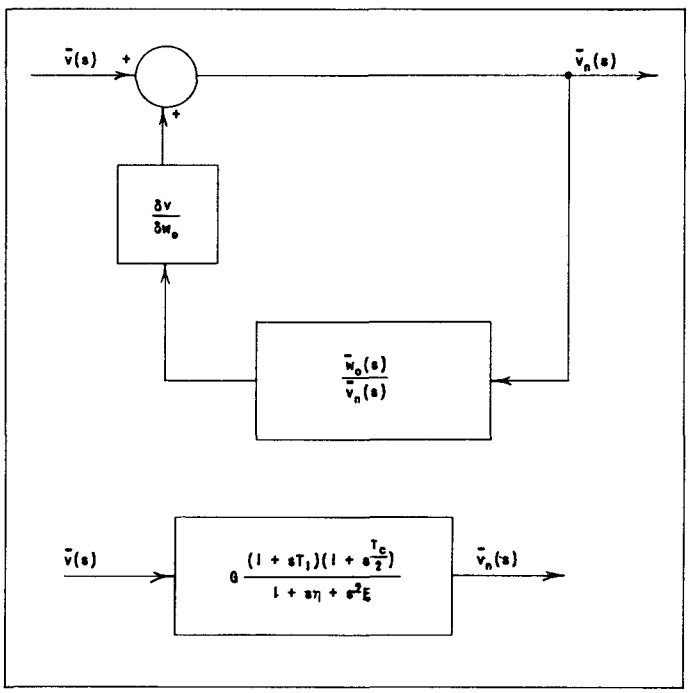

FIG. 13
EFFECT OF WATER ACCELERATION ON STEAM VOLUME

IX. STEAM MASS-PRESSURE RATE TRANSFER FUNCTION

The general form of this transfer function was derived in Reference 1, p. 25. The simplified form used in Section XI was obtained in Reference 6, p. 44. Nothing will be added in the present report to either of the above derivations.

X. THE EFFECT OF TEMPERATURE CHANGES

Power and pressure variations cause the temperatures in the various regions of the core to fluctuate. The reactivity effect produced by these temperature variations will now be considered.

A. Temperature Changes due to the Power Variations

Power variations affect the average fuel temperature and the subcooled water temperature in the nonboiling region. The temperature of the water-steam mixture in the boiling region is not directly influenced by the power variations, since the saturation temperature depends only on the pressure.

1. Fuel Temperature Effect

Transfer function between the nuclear power and the average fuel temperature is calculated with the aid of assumptions given in Section II:

$$\frac{\overline{\theta}_f(x,s)}{\overline{\nu}(x,s)} = \frac{R_1}{s\tau_1}\frac{d_1}{d_1+d_2}\left\{1-\left[\left(1-\frac{\rho_1 c_1}{\rho_2 c_2}\right)\left(\cosh\sqrt{\tau_2 s}+\frac{R_3}{R_2}\sqrt{\tau_2 s}\,\sinh\sqrt{\tau_2 s}\right)+\frac{\rho_1 c_1}{\rho_2 c_2}\right]\frac{\overline{\psi}(x,s)}{\overline{\nu}(x,s)}\right\}, \tag{75}$$

where $\theta_f(x,t)$ denotes the incremental value of the fuel temperature at x. Taking the single-time-constant approximation for $\overline{\psi}(x,s)/\overline{\nu}(x,s)$ from Eq. (4), expanding the hyperbolic functions into a Taylor series, and finally retaining only the first and the second terms, there is obtained

$$\frac{\overline{\theta}_f(x,s)}{\overline{\nu}(x,s)} = \frac{\left(\frac{R_1}{3}+R_2+R_3\right)d_1+\left(\frac{R_2}{2}+R_3\right)d_2}{d_1 d_2}\frac{1}{1+s\tau_f}, \tag{76}$$

where τ_f is given by Eq. (6).

The average fuel temperature can be obtained by integrating $\overline{\theta}_f(x,s)$ in the vertical direction. Ignoring the variation of R_3 in Eq. (76) as was done in Section II, and assuming a sinusoidal flux distribution and first-power flux weighting,

$$\frac{\bar{\theta}_f(s)}{\bar{n}(s)} = \frac{\pi^2}{8}\left(\frac{L'}{L}\right)\frac{d_1\left(\frac{R_1}{3}+R_2+R_3\right)+d_2\left(\frac{R_2}{2}+R_3\right)}{V_f\left(1+s\tau_f\right)} \quad . \tag{77}$$

This is the desired nuclear power-fuel temperature transfer function. The factor L'/L stems from the distinction between the actual and reduced core lengths, when calculating the actual volume V_f of all the fuel elements including the claddings.

2. Water Temperature Effect

Power variations in the nonboiling region produce fluctuations in the local water temperature. Denoting these fluctuations by $\theta_w(x,t)$ and using the energy balance equation, viz., Eq. (11), there is obtained

$$\frac{\partial\theta_w(x,t)}{\partial x}+\frac{1}{W_0^0}\frac{\partial\theta_w(x,t)}{\partial t}=\frac{q(x,t)}{c_w\dot{M}_t} \quad . \tag{78}$$

The average water temperature is calculated by integrating $\theta_w(x,t)$ in the whole channel with the weighting function $F(x)$. Obviously, $\theta_w(x,t) = 0$ in the boiling region.

Equation (78) has the same form as Eq. (18), which has already been solved. Then, the solution of Eq. (78) can be directly obtained from Eq.(23), which is the solution of Eq. (18):

$$\frac{\bar{\theta}_w(s)}{\bar{q}(s)}=\frac{1}{c_w\dot{M}_t}\frac{1}{L^2}\int_0^{L_{nb}}F(x)\,dx\int_0^{x}D(x')e^{-\frac{s}{W_0^0}(x-x')}\,dx'. \tag{79}$$

The explicit form of this transfer function for a sinusoidal flux distribution and first power flux weighting is similar to Eq. (28), provided the angle α is replaced by $\beta = \pi(L_{nb}/L)$. Hence, the following simplified transfer function is readily obtained:

$$\frac{\bar{\theta}_w(s)}{\bar{q}(s)}=\frac{1}{8\,c_w\dot{M}_t}\frac{(1-\cos\beta)^2}{1+s\tau_{qw}} \quad , \tag{80}$$

where

$$\tau_{qw} = 2\frac{(1-\cos\beta)^2}{\beta(2\beta-\sin 2\beta)}T_w \quad .$$

B. Temperature Changes due to Pressure Variations

Pressure changes cause the water temperature to fluctuate because the saturation temperature depends on the pressure.

In the boiling region, the water temperature immediately changes to its new value after a step change in the pressure. In the nonboiling region no immediate change occurs. The effect of a step pressure change is felt only upon the arrival of the recirculating water at the core inlet at the new saturation temperature. The recirculation time T_r'' from the saturation region in the downcomer to the core inlet is slightly less than the recirculation time T_r defined in Eq. (53). The difference is equal to the water transit time in the nonboiling region. No distinction will be made in the following between T_r'' and T_r, due to the uncertainty in the definition of both of them.

The transient behavior of the water temperature after the arrival of the recirculating water is the same as the one investigated in connection with variations of the boiling boundary. Although it could be easily taken into account, this transient will be disregarded on the ground that it lasts a very short time as compared to the recirculation time. This implies the assumption that the water temperature instantaneously rises at any point in the nonboiling region as soon as the recirculation water arrives at the core inlet.

With the above considerations, the pressure-water temperature transfer function can be obtained as

$$\frac{\bar{\theta}_w(s)}{\bar{p}(s)} = \frac{1}{L}\frac{d\Theta_s}{dP}\left[\int_{L_{nb}}^{L} F(x)\,dx + \frac{\dot{M}_r e^{-sT_r}}{\dot{M}_t}\int_{0}^{L_{nb}} F(x)\,dx\right] . \qquad (81)$$

In the case of sinusoidal weighting, Eq. (81) gives

$$\frac{\bar{\theta}_w(s)}{\bar{p}(s)} = \frac{1}{2}\frac{d\Theta_s}{dP}\left[(1-\cos\alpha) + (1+\cos\alpha)\, e^{-sT_r}\right] , \qquad (82)$$

where $\dot{M}_r/\dot{M}_t$ is replaced by 1 ($\dot{M}_r >> \dot{M}_{fw}$).

XI. REACTIVITY COEFFICIENTS

Three reactivity coefficients are needed to calculate the total feedback reactivity. These are fuel temperature, water temperature and void-reactivity coefficients. The following remark about the void-reactivity coefficient is true also for the other two.

The total reactivity Δk_v in voids can be calculated as

$$\Delta k_v = \alpha_v \int_0^L \sum_i V_i(x) F(x)\, dx \quad ,$$

where $V_i(x)$ is the steam volume per unit channel length about x, produced by the ith feedback mechanism. The factor α_v is the void-reactivity coefficient, defined as the reactivity per unit steam volume when the steam is uniformly distributed along the channel.

Since the weighted transfer functions, namely, $\int_0^L V_i(x)F(x)\, dx$, have always been considered throughout in this report, the total reactivity can be calculated by multiplying the sum of the transfer functions by α_v. The latter, however, may not be the coefficient one usually obtains from the experiments,[11] as explained in the following example:

Let the experimental reactivity coefficient be denoted by α_v'. Assume that it is calculated as the ratio of the reactivity change to the steam volume change. With the aid of the diagram shown in Fig. 14, where steady-state steam distribution is assumed to be linear, one obtains the following relation between α_v' and α_v:

$$\alpha_v = \alpha_v' \frac{1}{\pi} \left(\frac{L_b'}{L_b}\right)^2 \frac{\alpha^2}{\alpha - \sin\alpha} \quad . \tag{83}$$

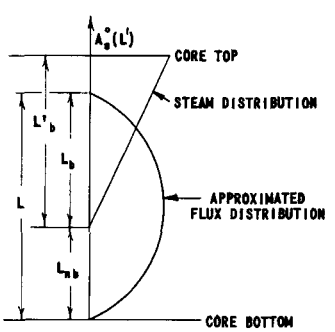

FIG. 14
CALCULATION OF CORRECTED VOID-REACTIVITY COEFFICIENT

The ratio L_b'/L_b comes from the difference between the actual and reduced core heights. The correction factor in Eq. (83) amounts to 1.75 for EBWR, where $\alpha = 2\pi/3$ and $L_b'/L_b = 1.2$.

As indicated by this example, the correction factor may be quite significant in certain applications. Therefore, care should be exercised to see that the proper value of the reactivity coefficient is being used.

XII. BLOCK DIAGRAM OF THE INHERENT FEEDBACK AND THE LIST OF FORMULAE

The complete block diagram for the inherent feedback in a natural-circulation boiling water reactor is depicted in Fig. 15. The expressions for the gains and the time constants are listed below:

Time Constants

τ_{fb}, τ_{fnb}: Fuel plate time constants in the boiling and nonboiling regions (Eq. 6):

$$\tau_f = \tau_1 \left[\frac{R_2 + R_3}{R_1} + \frac{1}{3} + \frac{\tau_2}{\tau_1} \left(\frac{1}{2} + \frac{R_3}{R_2} \right) \right]$$

τ_{qw}: Water temperature time constant (Eq. 80)

$$\tau_{qw} = 2 \frac{(1 - \cos \beta)^2}{\beta(2\beta - \sin 2\beta)} T_w$$

τ_{qv}: Power-void time constant (Eq. 30)

$$\tau_{qv} = \frac{2(1 - \cos \alpha)^2}{\alpha(2\alpha - \sin 2\alpha)} T_s \quad [\text{multiply by } 0.8 \text{ if } \alpha = (\tfrac{2}{3})\pi]$$

τ_{pv}: Pressure-void time constant (Eq. 50)

$$\tau_{pv} = \frac{2\alpha - 4 \sin \alpha + \sin 2\alpha + (K_1/K_2)(\alpha - \sin \alpha)}{2\alpha \left[2(K_1/K_2)(1 - \cos \alpha) - \sin^2 \alpha \right]} T_s$$

[K_1 and K_2 are given by Eqs. (47) and (48)]

τ_d: Steam mass-pressure rate time constant [Eqs. (4) and (5) in Reference 6, p. 44]

$$\tau_d = T_r \Bigg/ \left\{ 1 + \left[\frac{M_w}{H_s - H_w} \frac{dH_w}{dP} \Bigg/ \frac{M_s}{P} - \frac{M_s}{\Theta_s} \frac{d\Theta_s}{dP} + \frac{M_s}{H_s - H_w} \frac{dH_s}{dP} \right] \right\}$$

(Θ_s is in Rankine)

Gains

$$G_1, G_2 = \frac{\pi^2}{8V_f} \left(\frac{L'}{L} \right) \left[d_1 \left(\frac{R_1}{3} + R_2 + R_3 \right) + d_2 \left(\frac{R_2}{2} + R_3 \right) \right], \quad \text{(Eq. 77)}$$

$$G_3 = \frac{1}{4c_w \dot{M}_t} (1 - \cos \beta), \quad \text{(Eq. 80)*}$$

*Multiply by G_{10} to obtain the referred equation

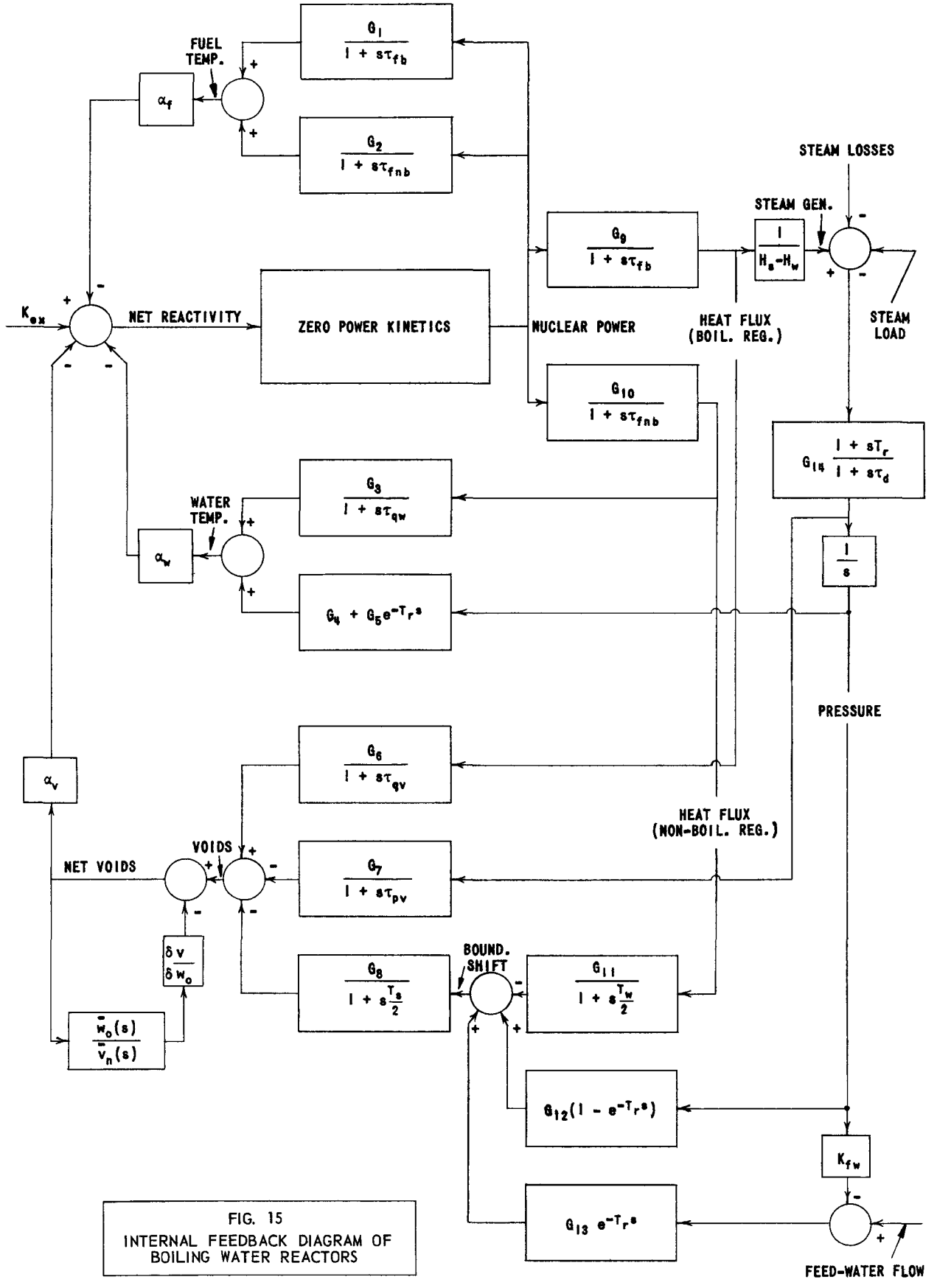

FIG. 15
INTERNAL FEEDBACK DIAGRAM OF BOILING WATER REACTORS

$$G_4 = \frac{d\Theta_s}{dP}\,\frac{(1-\cos\alpha)}{2}, \quad \text{(Eq. 82)}$$

$$G_5 = \frac{d\Theta_s}{dP}\,\frac{(1+\cos\alpha)}{2}, \quad \text{(Eq. 82)}$$

$$G_6 = \frac{\pi(1-\cos\alpha)}{4\,H_v\alpha}\,T_s, \quad \text{(Eq. 29)*}$$

$$G_7 = \frac{K_2}{4}(2\alpha - 4\sin\alpha + \sin 2\alpha) + K_1(\alpha - \sin\alpha), \quad \text{(Eq. 49)}$$

$$G_8 = -\frac{Q^0(L_{nb})}{H_v}\,\frac{\pi}{2}\,\frac{1-\cos\alpha}{\alpha}\,T_s, \quad \text{(Eq. 64)}$$

$G_9 = \frac{1-\cos\alpha}{2}$ (Power in the boiling region/Power in the whole channel)

$G_{10} = \frac{1+\cos\alpha}{2}$ (Power in the nonboiling region/Power in the whole channel)

$$G_{11} = -\frac{1}{Q^0(L_{nb})}, \quad \text{(Eq. 39)**}$$

$$G_{12} = \frac{dH_w}{dP}\,\frac{\dot{M}_t}{Q^0(L_{nb})}\,T_r, \quad \text{(Eq. 54)}$$

$$G_{13} = \frac{H_w - H_{fw}}{Q^0(L_{nb})}, \quad \text{(Eq. 55)}$$

$$G_{14} = 1\Big/\left[\frac{M_s}{P} - \frac{M_s}{\Theta_s}\,\frac{d\Theta_s}{dP} + \frac{M_s}{H_s - H_w}\,\frac{dH_s}{dP} + \frac{M_w}{H_s - H_w}\,\frac{dH_w}{dP}\right]$$

(Θ_s is in Rankine) [Eq. (5) in Reference 6, p. 44]

---

*Multiply by G_9 to obtain the referred equation

**Multiply by G_{10} to obtain the referred equation

XIII. APPLICATIONS

Two specific examples will now be considered to illustrate the application of the theoretical formulae derived in previous sections, and to check the validity of the assumptions: first, the power-void transfer function measurements performed at the Ramo-Wooldridge Research Laboratory,[12] on a boiling channel simulating the SPERT-IA reactor; secondly, the transfer function measurements[13] on EBWR at 20 Mw and 41 atm.

A. Power-void Transfer Function

The power-void transfer function measurements were made by modulating the channel power with 10% amplitude about the mean value (usually 500 watts) at a given frequency and measuring the amplitude and phase lag of the local void fraction at a given channel location. The experiment was repeated at different frequencies and channel locations to obtain the variation of the amplitude and phase with frequency and position. Details of the experimental technique and the results of the measurements are reported in Reference 12.

The flow diagram of the power-void transfer function is shown in Fig. 16. It is obtained from Fig. 15 by considering only the boxes designated by G_9, G_{10}, G_6, G_{11} and G_8. Pressure effects are eliminated, since the experiments were performed at constant atmospheric pressure.

The gain factors of the fuel plate transfer functions become $G_9 = L_b/L$ and $G_{10} = L_{nb}/L$, since the heat generation is uniform.

Heat flux-void transfer function is obtained from Eq. (23) by setting $D(x) \equiv 1$ and $F(x) \equiv 1$. The integration from L_{nb} to L in Eq. (23) is dropped because the local, instead of the integrated, steam volume is being considered here. The factor e^{-sT} represents the time delay associated with the bubble formation (see Section IV-A).

The heat flux-boiling boundary transfer function readily follows from Eq. (40).

The boiling boundary-void transfer function is obtained from Eq. (60) by setting $F(x) \equiv 1$ and by considering only the integrand.

The effect of the flow variations of the inlet water will not be considered in the overall power-void transfer function for the sake of simplicity. It is believed that such variations do not play any important role in the observed behavior of the power-void transfer function. The power-void transfer function is obtained from Fig. 16 as

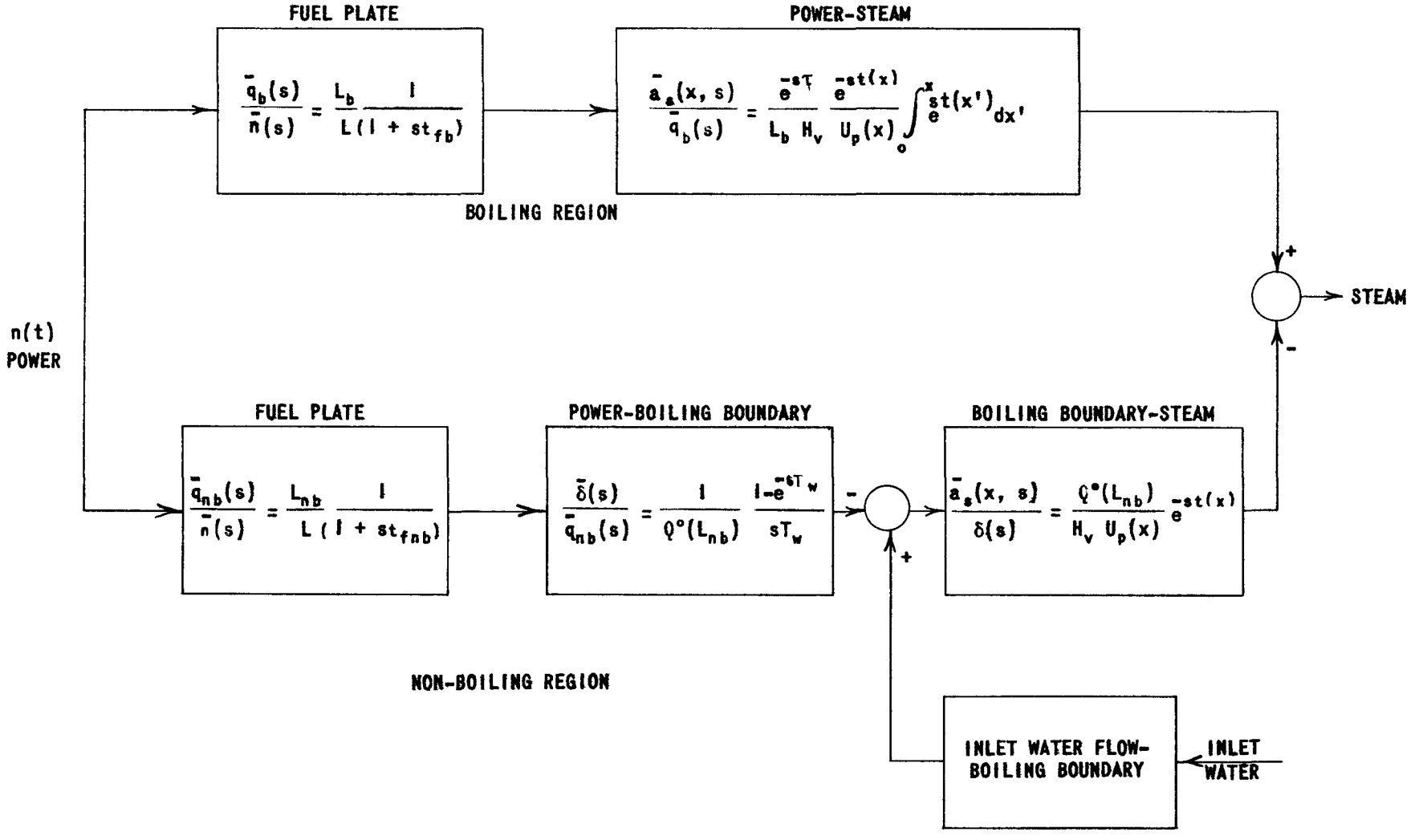

FIG. 16
BLOCK DIAGRAM OF POWER-VOID TRANSFER FUNCTION

$$\frac{\bar{a}_s(x,s)}{\bar{n}(s)} = \frac{1}{LH_v}\frac{e^{-st(x)}}{U_p}\left[\frac{e^{-s\tau}\int_0^x e^{st(x')}\,dx'}{(1+s\tau_{fb})} + \frac{L_{nb}}{(1+s\tau_{fnb})}\frac{1-e^{-sT_w}}{sT_w}\right], \quad (84)$$

where x is the distance from the boiling boundary.

The steam propagation velocity will be taken as $U_p = 2U^0(x)$, as explained in Section III.

The integral in Eq. (84) can be approximately evaluated by assuming that t(x) is proportional to x. Note that this assumption is made only in evaluating the integral.

The final form of the power-void transfer function is obtained from Eq. (84) as

$$\frac{\bar{a}_s(x,s)}{\bar{n}(s)} = \frac{e^{-j\pi ft(x)}}{2U^0(x)LH_v}\left\{\frac{x\ \mathrm{dif}\ ft(x)}{1+j2\pi f\tau_{fb}}\,e^{-j2\pi f\tau} + \frac{L_{nb}\ \mathrm{dif}\ fT_w}{1+j2\pi f\tau_{fnb}}\,e^{-j\pi f[T_w+t(x)]}\right\}, \quad (85)$$

where

$$\mathrm{dif}\ 2fT_w = \frac{\sin \omega T_w}{\omega T_w} \quad .$$

The following numerical values are taken from Reference 12:

L = 62.5 cm	Heated channel length
Lnb = 36 cm	Length of nonboiling region
x = 11 cm	Distance from the boiling boundary
A = 0.61 cm^2	Channel cross-sectional area
T_w = 0.74 sec	Water transit time in the nonboiling region
$U^0(x)$ = 260 cm/sec	Steam velocity at x = 11 cm
t(x) = 0.03 sec	Steam propagation time (this is half of the actual steam transit time of 0.06 sec)
ψ = 1.9 W/cm^2	Average heat flux (modulated by 10%); average power is 500 watts.
$H_v = 1.04(10^{-5})$ (W)(sec)/cm^3	Latent heat per unit volume of steam.

The fuel time constants τ_{fb} and τ_{fnb} are calculated from Eq. (6): τ_1 and R_1 are calculated as 7.89×10^{-3} sec and 4.15×10^{-2} $(cm^2)(°C)/watt$, respectively, for the aluminum fuel plates. The value of the incremental heat coefficient $(1/R_3)$ is obtained from Eqs. (2) and (3a) in the boiling region as $(1/R_{3b}) = 0.85$ watts/$(cm^2)(°C)$. The nonboiling heat transfer

coefficient is calculated from Dittus-Boelter equation, i.e., Eq. (3b), as $(1/R_{3nb}) = 0.46$ watts/(cm^2)(°C). These values are in good agreement with the experimental values given in Reference 12, p 67, which are 0.8 to 1.5 in the boiling region and 0.5 to 0.8 in the nonboiling region. Use of the average experimental values yields

$$\tau_{fb} = 0.20 \text{ sec}$$

and

$$\tau_{fnb} = 0.30 \text{ sec}$$

The time lag τ in Eq. (85) is taken as $\tau = 0.35$ sec for the reasons given later.

Use of the above numerical values in Eq. (85) yields the amplitude response shown in Fig. 17.

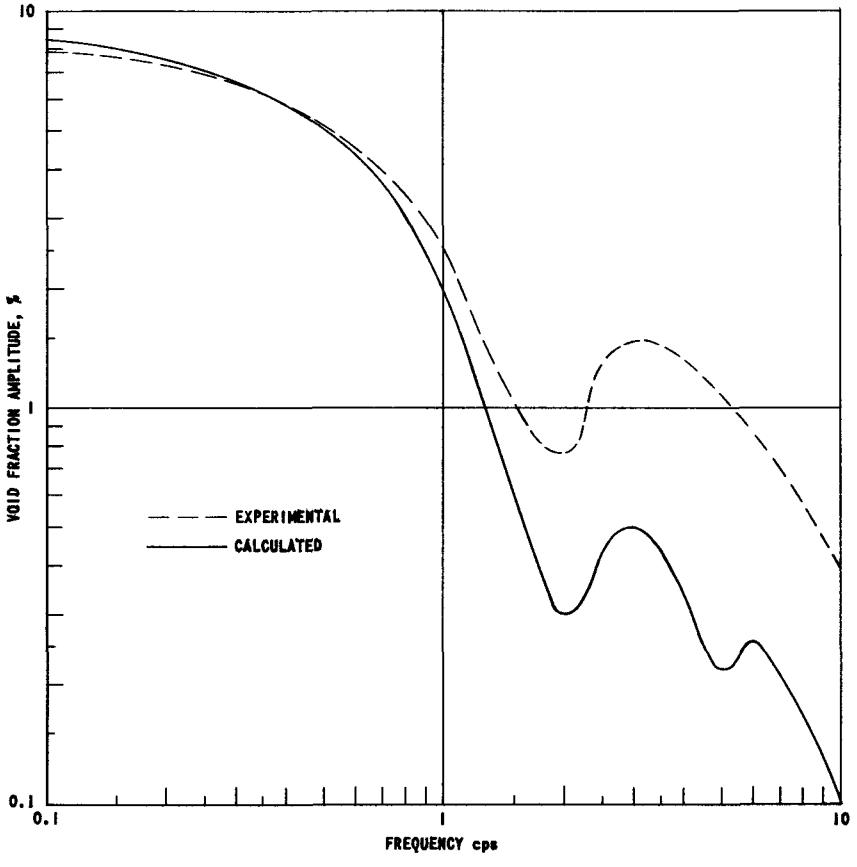

FIG. 17
AMPLITUDE RESPONSE OF POWER-VOID TRANSFER FUNCTION
(EXPERIMENTAL CURVE REPRODUCED FROM FIG. 11B2-2 OF REF. 12)

One observes that this curve is in good agreement with the experimental curve except for the high-frequency response. One finds, however, that the high-frequency response is very sensitive to the magnitude of the fuel time constant in the boiling region. Therefore, the agreement could be improved by suitable adjustment (by decreasing) of the fuel time constant, which is not accurately known anyway. Note that the frequency at which the node occurs coincides with the experimental value.

The high-frequency response of the power-void transfer function is determined only by the boiling region because the second term in Eq. (85), which represents the effect of the nonboiling region, becomes negligible at high frequencies as compared to the first term.

Spatial distribution of the amplitude at a constant frequency is shown in Fig. 18 for different frequencies. The variation of the steam velocity, which was needed in calculating the spatial distribution, was obtained from the void curve and the slip ratios given in Figs. 1 and 4 of Reference 15.

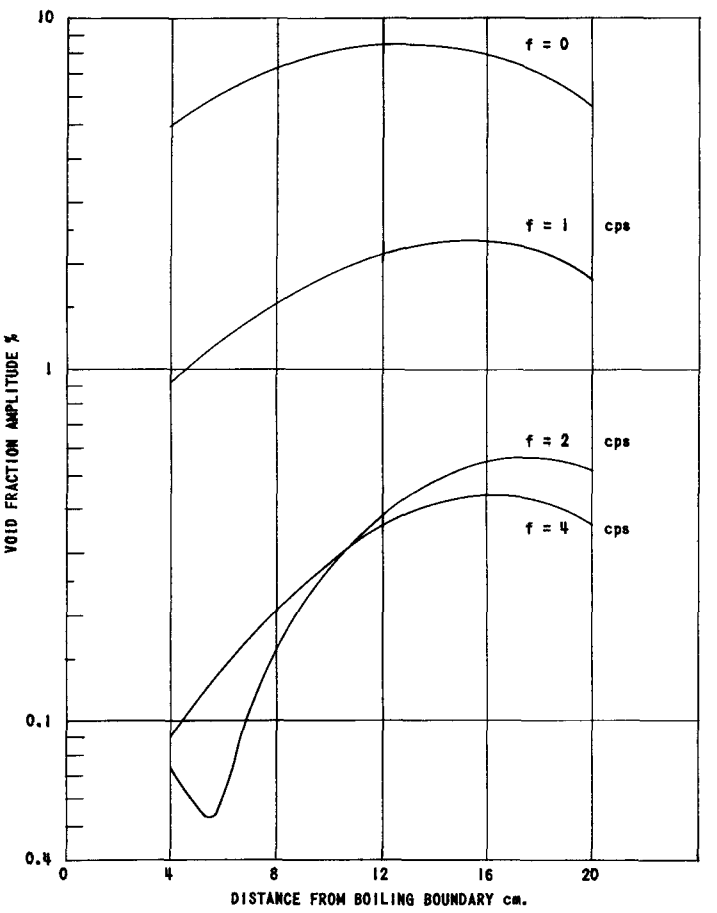

FIG. 18
AMPLITUDE DISTRIBUTION OF POWER-VOID TRANSFER FUNCTION

The shape of the amplitude distribution curve is determined by $(x + L_{nb})/U^0(x)$ at very low frequencies and by $x/U^0(x)$ at high frequencies. In the latter case, the effect of the second term in Eq. (85) is negligible, as mentioned before. In the intermediate frequency region, the shape of the amplitude curve depends on the relative phase and magnitude of the first and second terms in Eq. (85). If the phase difference happens to be approximately 180 degrees at the specified frequency, the amplitude curve possesses a node at a certain channel position (see Fig. 18, f = 2 cps).

The shapes of the amplitude distribution curves in Fig. 18 are in good agreement with the experimental curves given

in Fig. IIB2-6 of Reference 12. A quantitative comparison was impossible because the experiments were performed under different conditions. The predicted node is not observed at all in the experimental curves. This is probably due to the fact that the amplitudes were measured only at three channel positions at each frequency. The node might have been missed even if it really existed at an intermediate position. The predicted behavior may serve as a basis to check the validity of the proposed model.

The measured phase lag of the void response does not approach an asymptotic value, but increases approximately linearly with frequency (Fig. IIB2-3 of Reference 12). Such a behavior indicates the existence of a time lag in the system. This lag may be attributed to the time delay associated with the steam formation, as explained in Section IV A. Indeed, a slip ratio of 8-9, as reported in Fig. 4 of Reference 15 [see also Figs. 120 and 122 of Reference 14], and a bubble growth time of 40-50 milliseconds (p 634 of Reference 8) yield a delay of $\tau = 0.30\text{-}0.35$ sec, according to Eq. (25). This value checks well with the experimental value of $\tau = 0.30$ sec. However, this agreement cannot be regarded as conclusive because of the uncertainties involved in the bubble formation time.(16)

The distribution of the phase lag along the channel has some interesting features. One observes in Eq. (85) that the phase of the overall power-void transfer function is equal to the phase of the second term when x is sufficiently small. The phase of the second term varies between zero and $3\pi/2$ as explained in Appendix A. At high frequencies, where the second term is negligible, the phase lag is given by $-\left\{[2\tau + t(x)]\pi f + \tan^{-1}(\omega\tau_{fb})\right\}$. Hence, the phase lag will experience a rapid increase with the channel position, when the magnitude of the first term exceeds that of the second term. As an example, consider the case that f = 4 cps. The phase lag is approximately $-(3\pi/2)$ at x = 0, and -3.22π at x = 11 cm. This rapid change is observed on the corresponding experimental curve in Fig. IIB2-7 of Reference 12.

As a conclusion to this section, one may state that the theoretical power-void transfer function in Eq. (85) checks reasonably well with the experimental data presently available. However, this agreement is not sufficient to claim that the model represents the true description of the actual physical phenomena which take place in the boiling channel. More systematic experimental data must be collected in order to reach a definite conclusion.

B. EBWR Transfer Function

The technique and the results of the transfer function measurements on EBWR are presented in Reference 13. The comparison of the theoretical and experimental transfer functions has been made for operation at 20 Mw and 41 atm.

Table 1 in Appendix B contains the numerical values for the parameters needed in the analytical formulae. Table 2 contains the calculated values of the time constants and gains appearing in Fig. 15.

The block diagram shown in Fig. 15 can be rearranged as shown in Fig. 19 when the effects of the feedwater variations and the water acceleration are ignored. The parallel feedback paths corresponding to the temperature effects have also been disregarded in the numerical applications because their magnitudes are small in comparison with the magnitude of the void effects, except at very low frequencies.

The amplitude and the phase response of the closed loop transfer function have been computed on the IBM-704 using the (BUM) transfer function code (RE-132). The experimental and theoretical curves are depicted in Figs. 20 and 21. The difference between the experimental and calculated values is less than 5 decibels for the amplitudes, and 10 degrees for the phase angles in the frequency region of four decades. It can be noted that the discrepancy occurs mainly at low frequencies, where the closed-loop response is strongly dependent on the magnitude of the recirculation time T_r. The value of T_r was 9 sec in these calculations. This value was given as the best unbiased estimate from the theoretical calculations or out-of-pile measurements. The agreement at low frequencies might have been improved by properly adjusting (probably by increasing) the value of T_r, but a parameter study of this type is outside the scope of this report.

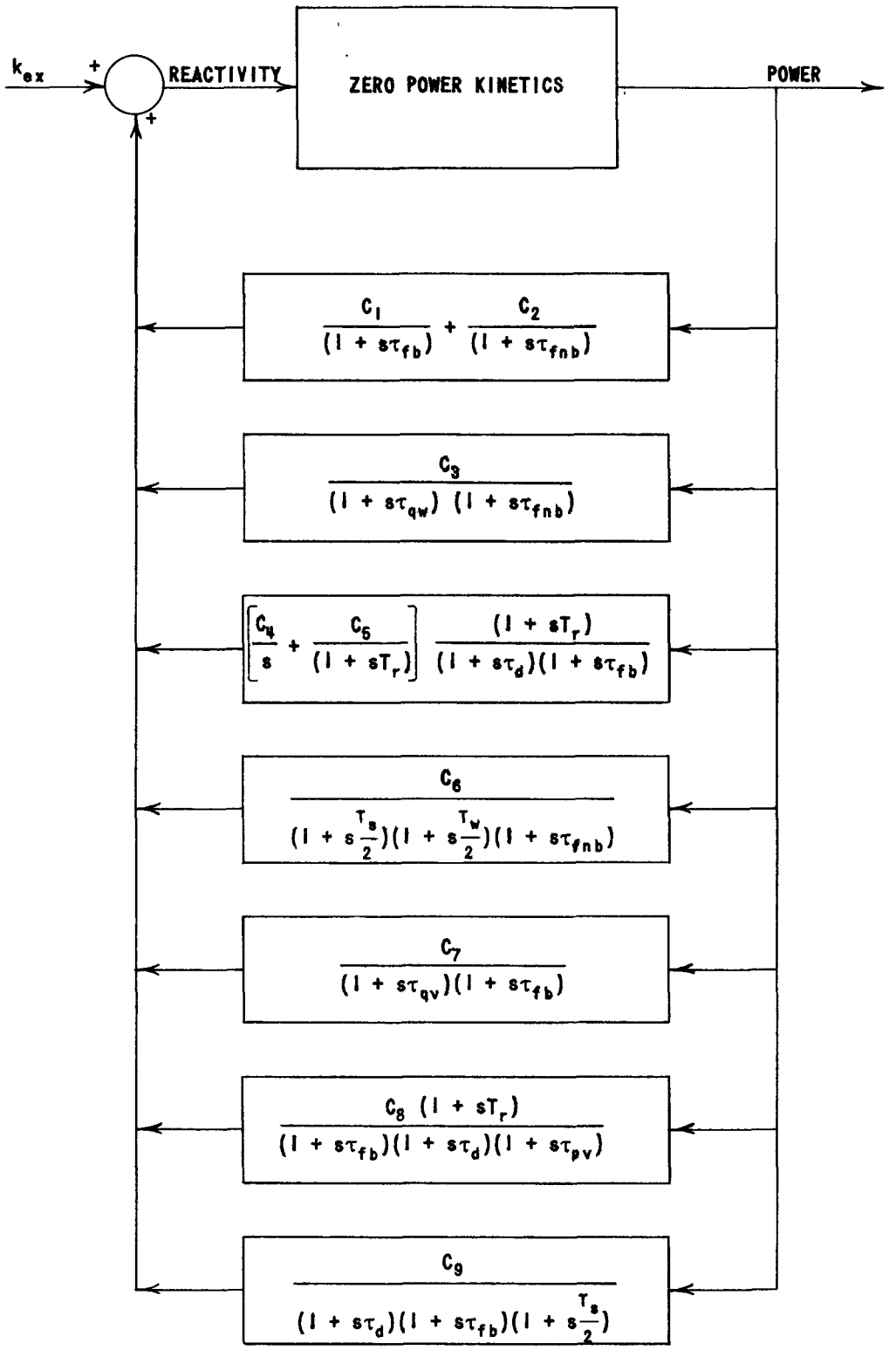

FIG. 19
BLOCK DIAGRAM OF PARALLEL FEEDBACK LOOPS

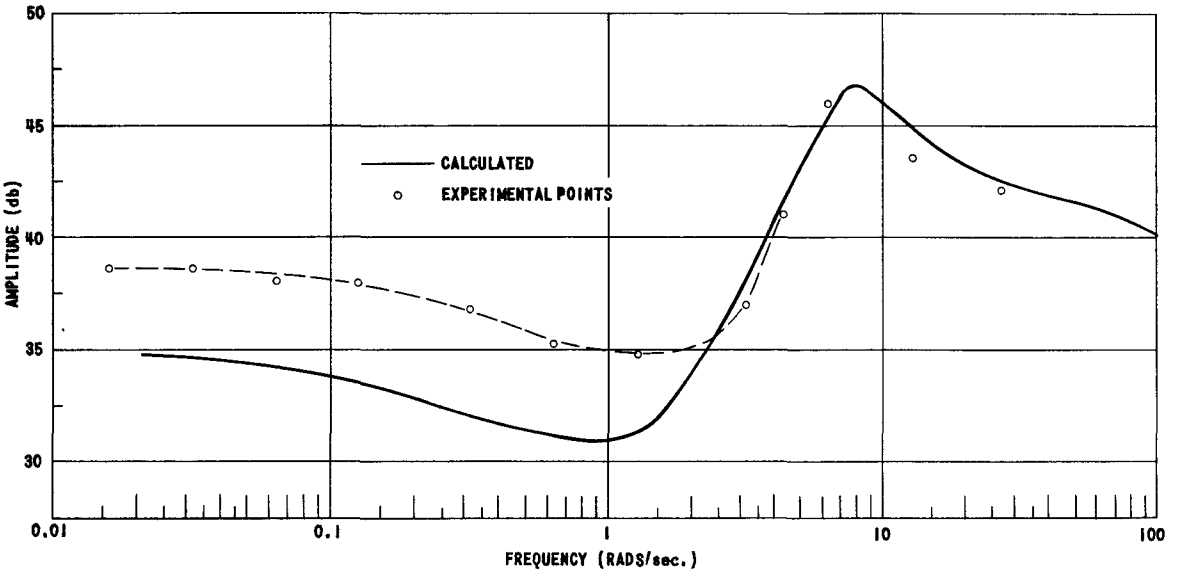

FIG. 20
AMPLITUDE RESPONSE OF EBWR TRANSFER FUNCTION
AT 20 Mw AND 41 atm

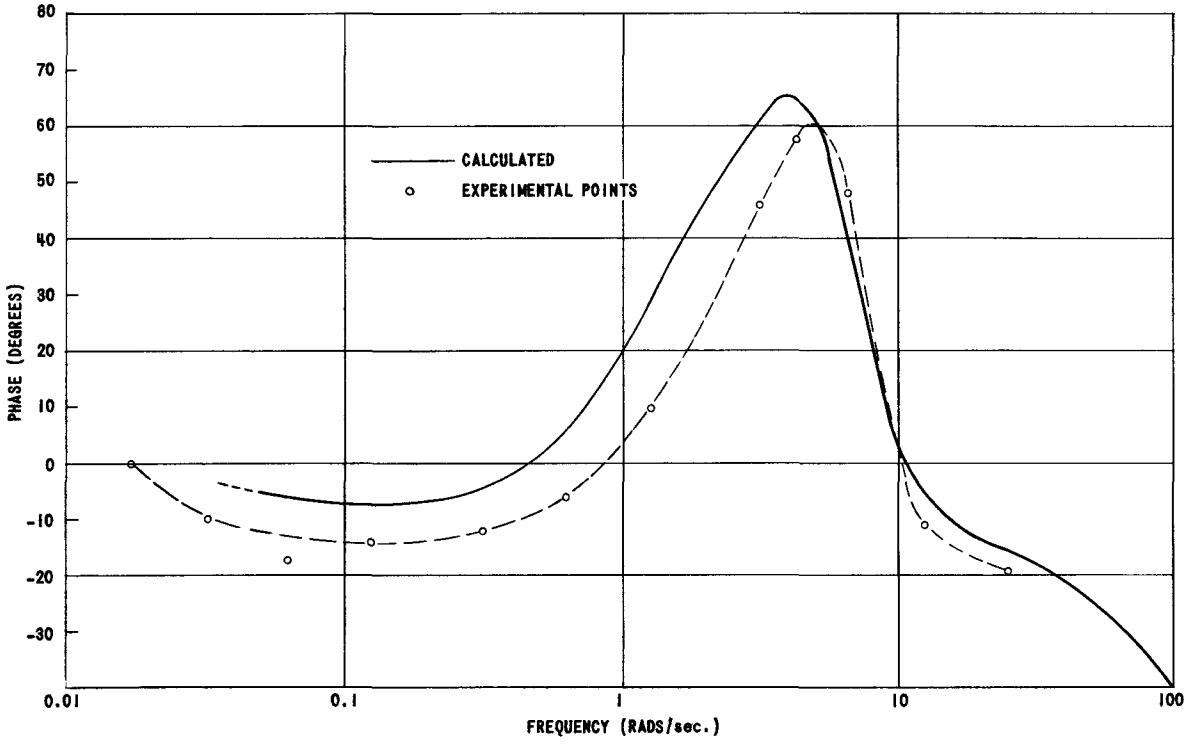

FIG. 21
PHASE RESPONSE OF EBWR TRANSFER FUNCTION
AT 20 Mw AND 41 atm

XIV. CONCLUSIONS

An attempt has been made in this report to investigate the internal feed-back mechanism of a boiling water reactor in a systematic and general way. The dynamic behavior of such reactors for small perturbations can be predicted in advance with the aid of the theoretical formulae derived in this report, if the numerical values of the quantities entering these formulae can be obtained from the basic calculations or from out-of-pile experiments.

The success of the theory in predicting the reactor response depends on the validity of the main assumptions as well as on the accuracy of the numerical values of the various parameters. Using the simplified transfer functions with single time constants instead of the exact expressions introduces another source of error. The magnitude of this error in some specific feedback mechanisms becomes as large as 4 db in amplitude at certain frequencies, as pointed out in the text. Therefore, it is difficult to know to what extent any observed discrepancy between the experimental and calculated reactor responses is due to the inadequacy of the assumption underlying the theory. More fundamental measurements, such as those investigated in Section XIII, are required to check the validity of the theoretical model.

In view of these uncertainties, the agreement obtained in the case of EBWR should be regarded as a confirmation of the analysis presented in this report.

APPENDIX A

DISTRIBUTED DELAY TRANSFER FUNCTION

The transfer function

$$Z(s) = \frac{1 - e^{-sT}}{sT} \tag{1A}$$

will be now investigated in more detail due to its frequent occurrence in the moderator dynamics. The time constant T in Eq. (1A) represents a transit time in general, such as the steam transit time and the water transit time. This transit time is usually different for the individual stream filaments in the channel due to the nonuniform distribution of the velocities across the channel. Therefore, an averaged transfer function ought to be defined.

Let the spread in the transit time be denoted by ΔT. By assuming a linear distribution in the range of ΔT, one may define an average transfer function as

$$Z(j\omega) = \frac{1}{2\ \Delta T} \int_{T - \Delta T}^{T + \Delta T} \frac{1 - e^{-j\omega T}}{j\omega T}\, dT = \frac{1}{j\omega T}\left[1 - \frac{\sin\ \omega\epsilon T}{\omega\epsilon T}\ e^{-j\omega T}\right] ,$$

where ϵ denotes the relative spread, viz., $\epsilon = \Delta T/T$.

The amplitude and the phase response of the average transfer function are plotted in Figs. 22 and 23 for two values of ϵ. Note that

$$Z(j\omega) = \frac{\sin(\omega T/2)}{(\omega T/2)}\ e^{-j\omega T/2}$$

when $\epsilon = 0$.

It is observed that the high-frequency response of $Z(j\omega)$ approaches $1/j\omega T$ for any nonzero value of ϵ. The low-frequency response, on the other hand, approaches $1/[1 + (j\omega T/2)]$. The latter is obtained by expanding the exponential term in Eq. (1A) into a Taylor series and retaining the first three terms.

When $Z(j\omega)$ is to be approximated by a single time constant, the value of the latter should be chosen according to the frequency region where more accuracy is desirable. If T is large, so that the break point in Fig. 22 is below the frequency region of interest, the time constant should be taken

as T [see Eq. (54)]. If T is small, so that the break point falls above the frequency region of interest, then the time constant (T/2) should be preferred. At any rate, single-time-constant representation is not satisfactory if the frequency region is large.

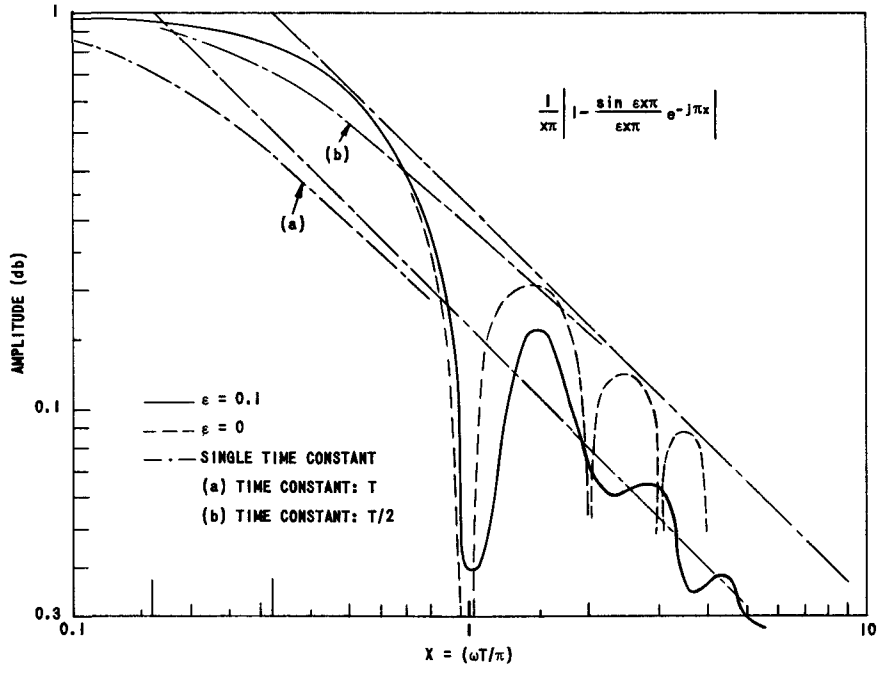

FIG. 22
AMPLITUDE RESPONSE OF DISTRIBUTED DELAY TRANSFER FUNCTION

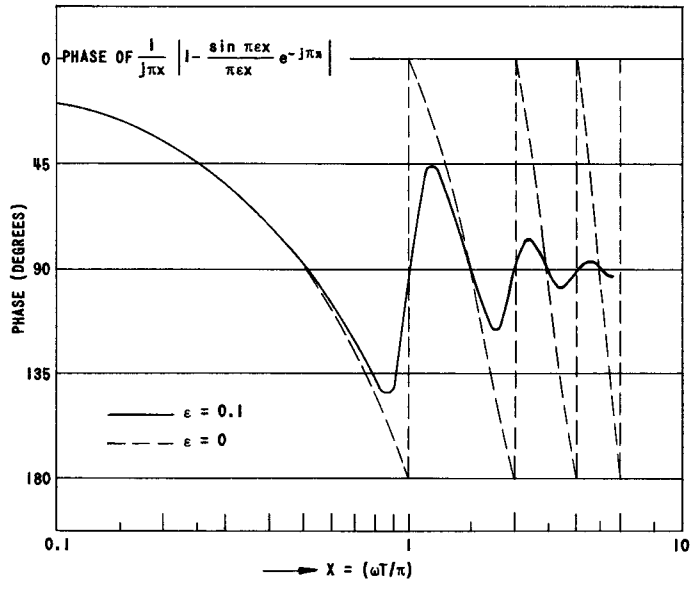

FIG. 23
PHASE RESPONSE OF DISTRIBUTED DELAY TRANSFER FUNCTION

APPENDIX B

NUMERICAL VALUES FOR EBWR AT 20 Mw AND 41 atm

Table 1

REACTOR PARAMETERS

A	$= 7831.5\ cm^2$	R_{3nb}	$= 7376\ (cm^2)(sec)(°C)/cal$
c_w	$= 1\ cal/(kg)(°C)$	T_r	$= 9\ sec$
c_1	$= 0.037\ cal/(kg)(°C)$	T_s	$= 0.35\ sec$
c_2	$= 0.069\ cal/(kg)(°C)$	T_w	$= 0.64\ sec$
d_1	$= 0.216\ cm$	$\dot{M}_t$	$= 476.3\ kg/sec$
d_2	$= 0.0488\ cm$	r	$= 2$
$H_w - H_{fw}$	$= 111.2\ cal/kg$	V_f	$= 493\ \ell$
H_v	$= 8.5\ 10^{-3}\ cal/cm^3$	W_0^0	$= 83.82\ cm/sec$
L'	$= 121.9\ cm$*	dH_w/dP	$= 7.096\ (kw)(sec)/(kg)(atm)$
L	$= 107.3\ cm$	dH_s/dP	$= 0.659\ (kw)(sec)/(kg)(atm)$
L_{nb}	$= 48.77\ cm$	dT_s/dP	$= 1.38\ °C/atm$
M_w	$= 8981.3\ kg$	λ	$= 6\ 10^{-5}\ sec^{-1}$
M_s	$= 326.6\ kg$	β	$= 0.0073$
R_1	$= 3647\ (cm^2)(sec)(°C)/cal$	α_f	$= -0.27\ cents/°C$
R_2	$= 1127\ (cm^2)(sec)(°C)/cal$	α_w	$= -2.9\ cents/°C$
R_{3b}	$= 365\ (cm^2)(sec)(°C)/cal$	α_v	$= -2.12\ cents/\ell$ **

*The reduced core height may be best determined by fitting a cosine curve with adjustable amplitude and wave length to the actual flux distribution by means of the least-square technique. However, the present value was obtained by graphical fitting in Fig. 6 as a rough estimate.

**This value has already been corrected for uniform distribution (see Section II).

Table 2

TIME CONSTANTS AND GAINS

$\tau_{fb} = 0.38$ sec	$G_3 = 3.88\ 10^{-3}$ °C/(cal)(sec)
$\tau_{fnb} = 0.44$ sec	$G_4 = 2.54\ 10^{-1}$ °C/(cal)(sec)
$\tau_{qw} = 0.25$ sec	$G_5 = 1.32\ 10^{-1}$ °C/(cal)(sec)
$\tau_{pv} = 0.03$ sec	$G_6 = 2.25\ 10^{-2}$ ℓ/(cal)(sec)
$\tau_{qv} = 0.11$ sec	$G_7 = -12.89$ ℓ/(atm)(sec)
$\tau_d = 1.46$ sec	$G_8 = -2.6$ ℓ/cm
$T_r/2 = 4.5$ sec	$G_9 = 0.65$
$T_s/2 = 0.175$ sec	$G_{10} = 0.34$
$T_w/2 = 0.32$ sec	$G_{11} = -1.23\ 10^{-2}$ cm/(cal)(sec)
$G_1 = 1.39\ 10^{-3}$ °C/(cal)(sec)	$G_{12} = 14.06$ cm/atm
$G_2 = 5.18\ 10^{-3}$ °C/(cal)(sec)	$G_{14} = 2.39\ 10^{-2}$ atm/kg

Table 3

GAINS OF THE PARALLEL FEEDBACK LOOPS

$C_1 = \alpha_f G_1$	$= -0.90\ 10^{-4}$ cents/kw
$C_2 = \alpha_f G_2$	$= -3.34\ 10^{-4}$ cents/kw
$C_3 = \alpha_w G_3 G_{10}$	$= -0.88\ 10^{-4}$ cents/kw
$C_4 = \alpha_w(G_4 + G_5) G_9 G_{14}/(H_s - H_w)$	$= -0.35\ 10^{-5}$ cents/kw
$C_5 = -\alpha_w T_r G_5 G_9 G_{14}/(H_s - H_w)$	$= -0.11\ 10^{-3}$ cents/kw
$C_6 = \alpha_v G_8 G_{10} G_{11}$	$= -1.46\ 10^{-2}$ cents/kw
$C_7 = \alpha_v G_6 G_9$	$= -1.39\ 10^{-2}$ cents/kw
$C_8 = \alpha_v G_7 G_9 G_{14}/(H_s - H_w)$	$= +0.48\ 10^{-3}$ cents/kw
$C_9 = \alpha_v T_r G_8 G_9 G_{12} G_{14}/(H_s - H_w)$	$= +1.16\ 10^{-2}$ cents/kw

APPENDIX C

REFINEMENTS IN THE TREATMENT OF PRESSURE EFFECTS

Should variations with pressure in steam density and in latent heat per unit steam volume be considered,* the fundamental equation, viz., Eq. (16), of the moderator dynamics takes the following form:

$$\frac{\partial(U_p a_s)}{\partial x} + \frac{\partial a_s}{\partial t} = \frac{q(x,t)}{H_v^0} - \frac{Q^0(x)}{(H_v^0)^2}\frac{dH_v}{dP}p(t) - \frac{1}{H_v^0}\left[A_s^0 \rho_s^0 \left(\frac{dH_s}{dP} + \frac{H_s^0 - H_w^0}{\rho_s^0}\frac{d\rho_s}{dP}\right) + \rho_w^0 A_w^0 \frac{dH_w}{dP}\right]\frac{dP}{dt} \quad , \quad (1C)$$

where H_v^0, ρ_s^0 and ρ_w^0 refer to the equilibrium values of latent heat per unit steam volume, steam density, and water density, respectively.

The effect of variations in H_v, viz., the second term on the right side of Eq. (1C), can be investigated using the proceedure followed in solving Eq. (18). One readily finds the pressure-void transfer function as

$$\frac{\bar{v}(s)}{\bar{p}(s)} = -\frac{Q^0}{H_v^0}\frac{dH_v}{dP}\left[\frac{\bar{v}(s)}{\bar{q}(s)}\right] \quad , \quad (2C)$$

where $[\bar{v}(s)/\bar{q}(s)]$ is the power-void transfer function given by Eq. (23) in the general case, and by Eq. (29) in the single time-constant approximation. The pressure-void transfer function will give rise to a new block in Fig. 15 from the pressure column to the input of the power-void transfer function marked by G_6 in the diagram. This block has a gain $(-Q^0/H_v^0)(dH_v/dP)\,G_9$ and no time constant. One can see that this new feedback link tends to decrease the total void volume when the reactor power tends to increase, and thus represents a positive reactivity effect. The low values of the calculated amplitude response in Fig. 20 at low frequencies may therefore be attributed to the neglect of this positive reactivity effect.

The variations in steam density with pressure appear in Eq. (1C) as a correction on the value of dH_s/dP. Therefore, it can be taken into account in the treatment of the pressure rate-steam void transfer function by replacing dH_s/dP in Eqs. (42), (47) and (48) with

$$\left(\frac{dH_s}{dP} + \frac{H_s^0 - H_w^0}{\rho_s^0}\frac{d\rho_s}{dP}\right) \quad . \quad (3C)$$

---

*The author is indebted to Mr. N. Suda at the IINSE for pointing out the possibility of variations in H_v.

However, this correction does not have any appreciable effect on the pressure rate-steam void transfer function, since it is small as compared to the term corresponding to the water enthalpy variations in Eqs. (47) and (48).

Finally, for the sake of completeness, one may add another block in Fig. 15, from the boiling boundary shifts to the steam generation point, to include the boiling boundary effects on the steam generation. It is readily seen that this block has a gain $[-Q^0(L_{nb})/(H_s-H_w)]$ and no time constant. Inclusion of this link, however, is not expected to influence the overall feedback transfer function appreciably.

ACKNOWLEDGMENT

The author gratefully acknowledges the valuable suggestions by J. A. Thie (Reactor Engineering Division), and wishes to express appreciation for the discussions and the assistance of F. Velona during the course of this work. The contribution by L. Palacios (Spain) to Section VII is also acknowledged.

REFERENCES

1. E. S. Beckjord, Dynamic Analysis of Natural Circulation Boiling Water Power Reactors, ANL-5799 (1958).

2. W. H. Jens and P. A. Lottes, Analysis of Heat Transfer, Burnout, Pressure Drop and Density Data for High Pressure Water, ANL-4627 (1951).

3. S. Glasstone, Principles of Nuclear Reactor Engineering, D. Van Nostrand, New York (1955) p. 678.

4. F. Narin and D. Langford, Analytic Solution for Transient Temperature Distributions in Two-region Nuclear Reactor Fuel Elements, Nuc. Sci. and Eng., 6, 386 (1959).

5. Z. Akcasu and J. A. Thie, Generalized Theory of Feedback, ANL-5849 (1959), Appendix E.

6. J. A. DeShong and W. C. Lipinski, Analyses of Experimental Power-Reactivity Feedback Transfer Function for a Natural Boiling Water Reactor, ANL-5850 (1958).

7. K. Oswatitisch, Gas Dynamics, Academic Press, New York (1956) p. 180.

8. Max Jakob, Heat Transfer, John Wiley, New York (1949), Vol. I, p. 624.

9. J. A. Fleck, The Dynamic Behavior of Boiling Water Reactors, Reactor Science (J. Nuclear Energy), 11, 114 (1960).

10. P. A. Lottes and W. S. Flinn, A Method of Analysis of Natural Circulating Boiling Systems, Nuc. Sci. and Eng., 1, 461 (1956).

11. J. A. Thie, EBWR Physics Experiments, ANL-5711 (1957) p. 10.

12. Kinetic Studies of Heterogeneous Water Reactors, Annual Summary Report - 1959, Ramo-Wooldridge Research Laboratory, California (1960).

13. J. A. DeShong, Jr., Power Transfer Functions of EBWR Obtained Using a Sinusoidal Reactivity Driving Function, ANL-5798 (1958).

14. The EBWR, Experimental Boiling Water Reactor, ANL-5607 (1957).

15. Kinetic Studies of Heterogeneous Water Reactors, Progress Report No. 16, Ramo-Wooldridge Research Laboratory, California (September 30, 1959).

16. S. G. Bankoff and R. D. Mikesell, Bubble Growth Rates in Highly Subcooled Nucleate Boiling, Second National Heat Transfer Conference, Chicago (August 1958).